

GANs for Medical Image Analysis

Salome Kazemina^{a,1}, Christoph Baur^{b,1}, Arjan Kuijper^c, Bram van Ginneken^d, Nassir Navab^b, Shadi Albarqouni^b, Anirban Mukhopadhyay^a

^a*Department of Computer Science, TU Darmstadt, Germany*

^b*Computer Aided Medical Procedures (CAMP), TU Munich, Germany*

^c*Fraunhofer IGD, Darmstadt, Germany*

^d*Radboud University Medical Center, Nijmegen, The Netherlands*

Abstract

Generative Adversarial Networks (GANs) and their extensions have carved open many exciting ways to tackle well known and challenging medical image analysis problems such as medical image de-noising, reconstruction, segmentation, data simulation, detection or classification. Furthermore, their ability to synthesize images at unprecedented levels of realism also gives hope that the chronic scarcity of labeled data in the medical field can be resolved with the help of these generative models. In this review paper, a broad overview of recent literature on GANs for medical applications is given, the shortcomings and opportunities of the proposed methods are thoroughly discussed and potential future work is elaborated. We review the most relevant papers published until the submission date. For quick access, important details such as the underlying method, datasets and performance are tabulated. An interactive visualization which categorizes all papers to keep the review alive, is available at http://livingreview.in.tum.de/GANs_for_Medical_Applications/.

Keywords: Generative Adversarial Networks, Deep learning, Medical imaging, Survey

1. Introduction

From the early days of Medical Image Analysis, Machine Learning (ML) and Artificial Intelligence (AI) driven systems have been a key component for complex decision making - a brief history of which can be found in (Litjens et al., 2017). Across generations of development, the focus was mostly on decision making at different granularity levels. These techniques range from low-level

Email addresses: salome.kazemina@gris.tu-darmstadt.de (Salome Kazemina), c.baur@tum.de (Christoph Baur), arjan.kuijper@mavc.tu-darmstadt.de (Arjan Kuijper), bram.vanginneken@radboudumc.nl (Bram van Ginneken), navab@cs.tum.edu (Nassir Navab), shadi.albarqouni@tum.de (Shadi Albarqouni), anirban.mukhopadhyay@gris.tu-darmstadt.de (Anirban Mukhopadhyay)

¹The authors contributed equally to this work.

pixel processing over feature engineering combined with supervised classifier learning to the recent wave of feature learning using Convolutional Neural Networks (CNNs).

Until recently, the driving focus of the Medical Image Analysis (MIA) community has been on the supervised learning of decision boundaries, while generative tasks have been on the back seat. This changed dramatically with the advent of Generative Adversarial Networks (GANs) (Goodfellow et al., 2014a), which lead to a new age of generative modeling and distribution learning. With their abilities to mimic data distributions and to synthesize images at yet unprecedented levels of realism, GANs have carved open new ways to bridge the gap between *supervised learning* and *image generation*.

The mentioned improvements are essentially due to the following properties: 1) GANs maximize the probability density over the data generating distribution by exploiting density ratio estimation (Isola et al., 2017) in an indirect fashion of supervision; 2) GANs can discover the high dimensional latent distribution of data, which has lead to significant performance gains in the extraction of visual features.

This review summarizes GAN-based architectures proposed for medical image processing applications published until the end of 2018.

We categorized the reviewed papers into 7 categories according to the following applications: synthesis, segmentation, reconstruction, detection, de-noising, registration, and classification. The categorical distribution of the reviewed papers can be seen in Figure 1. Methods based on GANs were applied to a variety of different medical imaging modalities such as MRI (Magnetic Resonance Imaging), CT (Computed Tomography), OCT (Optical Coherence Tomography), chest X-Ray, Dermoscopy, Ultrasound, PET (Positron Emission Tomography) and Microscopy.

To find the papers we searched for the keywords medical and GAN (or generative adversarial network) along with the aforementioned applications in Google Scholar, Semantic Scholar, PubMed, and CiteSeer. Also, we checked references and citations of selected papers. Since GANs are rather new, and a significant number of articles are still in the publication process of different journals and conferences, we covered pre-prints published in arXiv as well.

For quick access, we summarized key information on the reviewed methods, such as metrics, datasets, image modality and the employed architectures in Tables. Also, we provide a live tree at http://livingreview.in.tum.de/GANs_for_Medical_Applications/ for ease of categorization of papers. Further, we thoroughly discuss the advantages and shortcomings of the methods and specify clear directions for future work.

We thus ended up with 77 papers which we consider the most relevant ones covering a broad spectrum of applications and variety of GANs. The remainder of this paper is structured as follows:

In Section 3, we introduce the architecture of the GAN and its subclasses which are used in medical image applications. In Section 4, different contributions of GANs in medical image processing applications (de-noising, reconstruction, segmentation, registration, detection, classification, and synthesis)

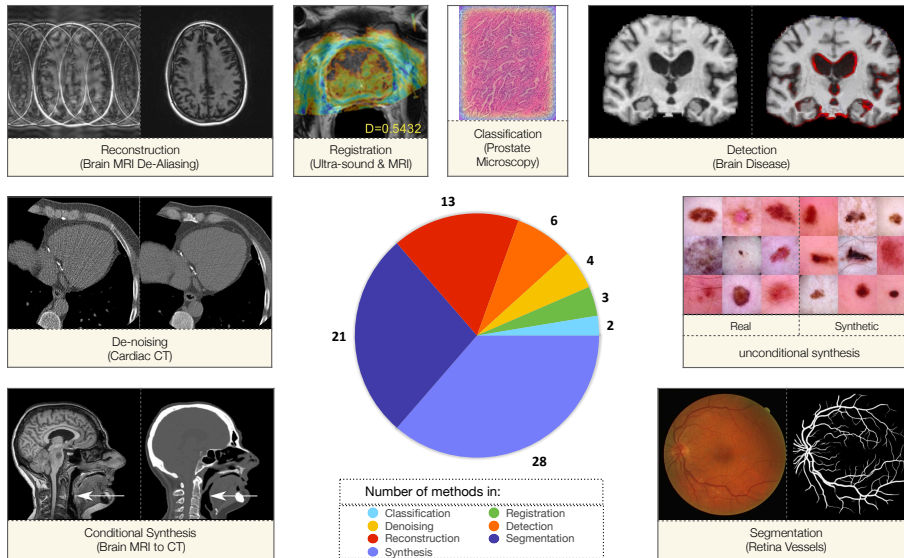


Figure 1: The pie chart of distribution of papers and visual examples of GAN functionality among the different applications. Examples are taken from papers as the following: Conditional synthesis Wolterink et al. (2017a), Denoising Wolterink et al. (2017b), Reconstruction Zhang et al. (2018), Registration Yan et al. (2018), Classification Ren et al. (2018), Detection Baumgartner et al. (2018), Unconditional synthesis Baur et al. (2018b), and Segmentation Son et al. (2017).

are described and Section 5 provides a conclusion about the investigated methods, challenges and open directions for the employment of GANs in medical image processing.

2. Opportunities for Medical Image Analysis

Supervised Deep Learning is currently the state of the art in many Computer Vision and Medical Image Analysis tasks, but its success is heavily dependent on the large-scale availability of labeled training data. In the medical field, this is a fundamental problem as often there is a severe lack of labeled data. This *data scarcity* arises from the tedious, time-consuming and costly nature of medical image acquisition and labeling. Furthermore, in the medical field, many datasets suffer from severe *class imbalance* due to the rare nature of some pathologies. GANs can potentially alleviate these two limitations by generating realistic-looking images from an implicit distribution that follows the real data distribution. The community has recognized this potential early and has been eagerly investigating GAN's suitability for tackling these problems. Applied research on GANs for such medical image synthesis can be broadly classified into two categories: i) Unconditional and ii) Conditional Image Synthesis. The GAN is originally an unconditional, unsupervised generative model which generates data from noise and leaves the user with limited influence on the generated

output (a review of such methods can be found in Subsection 4.1.1). Conditional variants have also been proposed, which allow to seed the generation process with prior information such as class labels, image attributes or even images themselves (see Subsection 4.1.2).

While labeled data might be scarce in the medical field, unlabeled data is often readily available. To leverage both labeled and arbitrary amounts of unlabeled data, numerous so-called *Semi-Supervised Deep Learning* methods have been proposed throughout the last years. Recent advances in this field make use of adversarial networks, the core-concept behind GANs, to harness both labeled and unlabeled data in the training of classifiers and segmentation models. A related issue hampering Deep Learning is the effect of so-called *domain shift*, i.e. a shift between the training and testing data distribution. Such a shift frequently occurs in the medical field and often leads to models that generalize poorly beyond the training data, with potentially unpredictable behavior. Prominent examples are i) MR data, where images from different device vendors exhibit very different characteristics, or ii) histopathological images, which vary greatly due to different staining protocols and equipments. GAN-based Domain Adaptation methods have recently shown great potential to close this gap, some of which are reviewed in Subsection 4.2 and 4.7.

This potential comes primarily from the introduction of an adversarial network into the overall optimization process. According to Odena et al. (2017), such a network can be understood as a learned, rich similarity metric: Traditional similarity metrics such as the ℓ_1 or ℓ_2 -distance are known to produce blurry results and lack the incorporation of spatial context, whereas such a learned similarity metric allows to optimize for concepts in images beyond the pixel level. This appealing property has recently been exploited in medical image denoising (see Subsection 4.5), superresolution, image-to-image translation (see Subsection 4.1.2) and even medical image segmentation (see Subsection 4.2).

The newly achieved levels of realism promoted by adversarial networks also open up new opportunities for tackling problems with high time-complexity, such as medical image reconstruction or registration. These problems are mathematically well modeled, but usually require a costly iterative optimization. GANs have been successfully used to learn a mapping from raw signals to reconstructed images (see Subsection 4.3) or to register medical images (see Subsection 4.6) in a single forward pass while ensuring coherence and high levels of realism.

3. Basic GAN models employed in medical applications

In this section, we introduce the general concept behind GANs, their conditional variants as well as a variety of prominent extensions. These extensions comprise the DCGAN, Markovian GAN, conditional GAN, CycleGAN, Auxiliary Classifier GAN, Wasserstein-GAN as well as Least Squares GAN which are used as the inspiring models in medical applications.

In the context of this work, there are three *Adversarial* concepts, which should be understood properly by their different meanings. *Adversarial attack* means to make imperceptible changes to an image such that a classifier misclassifies it. Usually, the modified image, called adversarial image or *adversarial examples* (Goodfellow et al., 2014b), is not distinguishable from the original image visually (Szegedy et al., 2013). *Adversarial training* proposed by Szegedy et al. (2013) is an idea that increases the robustness of neural networks against adversarial attacks by training the model with both normal and adversarial examples. Due to the state of existing neural networks at that time, implementing adversarial training was not a practical solution. The effectiveness of this idea became apparent when Goodfellow et. al employed it in GANs (Goodfellow et al., 2014a).

3.1. GAN

The GAN framework (Goodfellow et al., 2014a) consists of a training dataset \mathbf{X} , whose underlying distribution we denote p_{real} , and a pair of competing networks: a generator (G) with parameters θ_G , and a discriminator (D) with weights θ_D (see Figure 2). G aims to find a mapping $\hat{x} = G(z; \theta_G)$ that maps latent random variables $z \sim p_z(z)$ —drawn from a prior distribution p_z —to generated data $\hat{x} \in \hat{\mathbf{X}}$, which is supposed to follow the distribution $p_\theta(\hat{x}|z)$. The primary goal is to optimize this mapping such that the distribution of generated data $\hat{\mathbf{X}}$ resembles the distribution of the training data \mathbf{X} , i.e. $p_\theta(\hat{x}|z) \sim p_{real}$. In other words, G is supposed to generate fake data which must not be distinguishable from real data. This is achieved with the help of the discriminator network D, whose task is to classify between fake and real samples. Essentially, D is a binary classifier which yields $D(x) = 1$ for real samples and $D(\hat{x}) = 0$ for fake data. Both networks are adversaries as G attempts to gradually synthesize more and more realistic samples which D would misclassify as real, while D constantly learns to differentiate between real and synthesized samples. Mathematically speaking, D and G play a two-player minimax game with the following value function $V(G, D)$:

$$\min_G \max_D V(D, G) = \mathbb{E}_{x \sim p_{data}(x)} [\log(D(x))] + \mathbb{E}_{z \sim p_z(z)} [1 - \log(D(G(z)))] \quad (1)$$

To optimize for Equation 1, D is trained to maximize the probability of correct label assignment for fake and real data, while G is trained to trick D into thinking a generated sample is real by minimizing $\log(1 - D(G(z)))$. In practice, these networks are implemented as Multi-Layer Perceptrons (MLPs) and usually trained with minibatch stochastic gradient descend in an alternating fashion. Once trained, it is sufficient to sample a random z and feed it through the generator in order to synthesize data. This *adversarial training* framework exhibits a few interesting properties: 1) the generator G is updated only through gradients back-propagated from the discriminator and 2) no explicit correspondences between z , x and \hat{x} are required, such that input is not explicitly memorized by G. 3) Furthermore, as proven by the authors, optimization for Equation 1

minimizes the Jensen-Shannon (JS) divergence between the distributions of real and synthetic data.

Although theoretically well grounded, the vanilla GAN has proven to be quite hard to train. General convergence is heavily dependent on hyper-parameter tuning to avoid vanishing or exploding gradients, and they are prone to *mode collapse*. This term describes a phenomenon where GANs map all z to very similar synthetic samples covering only a single mode of the data distribution. During optimization, these modes might also change (so-called *mode hopping*). A plethora of extensions and subclasses have been proposed to cope with these problems, a selection which is introduced in the following subsections.

3.2. DCGAN:

To address the instability of the basic GAN architecture and increase the resolution of synthesized images, Radford et al. (2015) propose the Deep Convolutional GAN (DCGAN). In this model, both the generator and discriminator follow a deep convolutional network architecture, exploiting the efficacy of spatial kernels and hierarchical feature learning. Concepts such as Batch-Normalization and Leaky-ReLU have been included to improve training stability, but issues such as mode collapse were not entirely resolved.

3.3. cGAN:

Since in the original GAN no control on the actual image generation is given, Mirza and Osindero (2014) proposed the conditional GAN (cGAN) to incorporate additional information like class labels in the image generation process (Figure 3). In the cGAN, the generator is presented with random noise z jointly with some prior information c . Additionally, the prior knowledge c is fed into the discriminator together with the corresponding real or fake data. Mathematically speaking, the cGAN framework is given as follows:

$$\min_G \max_D V(D, G) = \mathbb{E}_{x \sim p_{data}(x)} [\log(D(x|c))] + \mathbb{E}_{z \sim p_z(z)} [1 - \log(D(G(z|c)))] \quad (2)$$

The authors showed that conditioning the GAN not only improves the generation of detailed features in the target image but also helps training stability.

Another conditional GAN framework is the Markovian GAN (MGAN) (Li and Wand, 2016), proposed for fast and high-quality style transfer. The MGAN, as depicted in Figure 4, heavily utilizes a pre-trained VGG19 network with fixed weights to extract high-level features for both style transfer and preserving the image content. Both the discriminator and generator network are prepended with a VGG19 network to extract feature maps. An additional perceptual loss on those extracted feature maps forces the generator to generate images with realistic VGG19 feature activations—as would have been obtained on real data.

Isola et al. (2017) proposed Pix2Pix, a very successful variant of the cGAN for high-resolution image-to-image translation. The Pix2Pix generator follows the U-Net (Ronneberger et al., 2015) architecture, while the discriminator—similar to MGAN—follows a fully convolutional architecture for differentiating between the real and fake high resolution data. The authors showed that the skip

connections within the U-Net generator are very beneficial for global coherence of the synthesized images. In contrast to the original GAN framework, Pix2Pix requires pairs of corresponding input and desired output images, though. This allows the use of the ℓ_1 loss between the generators' output and actual ground-truth image to stabilize the training.

3.4. *cycleGAN*:

For image transformation between two domains, the model should be able to extract characteristic features of both domains and to discover the underlying relationship between those. Zhu et al. (2017) proposed the CycleGAN to provide these principles. In essence, the framework combines two GANs to find a mapping from domain X to domain Y and vice versa. These consist of a generator $G : X \rightarrow Y$, trained by discriminator D_Y , and generator $F : Y \rightarrow X$, trained by discriminator D_X (Figure 5). The two GANs are chained together and a cyclic loss function forces them to reduce the space between their possible mapping functions. More precisely, this cyclic loss function minimizes the discrepancy between the original image and the reconstruction obtained from the chained generators. The final loss function of cycleGAN is defined as:

$$L(G, F, D_X, D_Y) = L_{GAN}(G, D_Y, X, Y) + L_{GAN}(F, D_X, Y, X) + \lambda L_{cyc}(G, F) \quad (3)$$

with

$$L_{cyc}(G, F) = \mathbb{E}_{x \sim P_{data}(x)}[\|F(G(x)) - x\|_1] + \mathbb{E}_{y \sim P_{data}(y)}[\|G(F(y)) - y\|_1] \quad (4)$$

3.5. *AC-GAN*

The Auxiliary Classifier GAN (AC-GAN) proposed by Odena et al. (2017) describes a different approach towards constructing a GAN conditioned on classes. Authors report that instead of providing both the generator and the discriminator networks with prior information (as shown in the cGAN), the discriminator can be additionally tasked with respectively classifying its input. More precisely, the discriminator architecture is modified such that after a few layers it splits into a standard discriminator network as well as an auxiliary classifier network (see Figure 6), which aims at classifying samples into different categories. According to the authors, this allows to use (partially) pre-trained discriminators and appears to stabilize training.

3.6. *WGAN*:

In the discussed frameworks, the data distributions of generated and real images are matched by means of the Jensen-Shannon (JS) divergence. This divergence measure potentially makes gradients vanishing and the saddle-point of optimization unreachable, which are the underlying reasons behind GAN failures. Arjovsky et al. (2017) proposed the Wasserstein-GAN (WGAN) which uses the Earth Mover (ME) or Wasserstein-1 distance as a more optimal divergence measure to avoid vanishing gradients. This model has proven to be much more robust, while easy to implement. In practice, the downside of the WGAN is its slow optimization.

3.7. LSGAN:

Mao et al. (2017) also tried to tackle the training instability of GANs with their so-called Least Squares GAN (LSGAN). Similarly to WGAN, the loss function is modified to avoid vanishing gradients:

$$\min_G \max_D V(D, G) = \mathbb{E}_{x \sim p_{data}(x)} [(D(x) - b)^2] + \mathbb{E}_{z \sim p_z(z)} [(D(G(z))) - a]^2 \quad (5)$$

This loss-function operates directly on the logits of the discriminator network, where $a = 0$ and $b = 1$ are the controlling parameters for fake and real data, respectively. This way, the fake images which are discriminated as real, even if they are far away from the dense distribution of real data, will be penalized more during optimization. On the other hand, the gradient faces the least value only if the distribution of fake data perfectly matches the distribution of real data.

4. Applications in Medical Image Processing

In this section, we summarize GAN-based methods which are proposed to solve medical imaging problems in 7 application categories: synthesis, segmentation, reconstruction, detection, de-noising, registration and classification. In every subsection, a table summarizes the most important details in reviewed methods: the basic architectures and loss functions proposed, image modality and dataset properties, the evaluated performance of the proposed method, and if the paper underwent peer-review (PR) or provided any source code. Since various metrics are used for evaluation of different methods, we provided Table 1 to explain metrics briefly.

4.1. Synthesis

Originally, GANs have been proposed as an entirely unsupervised generative framework, with the ability to map from random noise to synthetic, realistically looking images. With the conditional GAN, the framework has also been successfully turned into a supervised generative framework by conditioning on prior knowledge, rather than noise alone. For clarity, we refer to the original GAN framework as the *unconditional* or *unsupervised* GAN, in contrast to the *conditional* GAN. The generative property of both frameworks has been exploited in various ways for synthesizing certain types of medical images. In the following, a broad overview on works from both categories will be given. In the particular case for conditional approaches, we further classify the contributions based on the image modality.

4.1.1. Unconditional Image Synthesis:

A great variety of works has recently appeared in the field of unsupervised medical image generation using GANs, which allows to tackle problems such as data scarcity and class imbalance (Frid-Adar et al., 2018), facilitates data

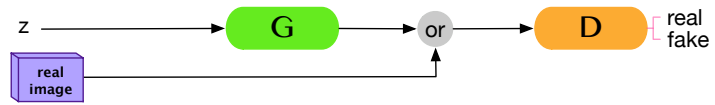


Figure 2: GAN

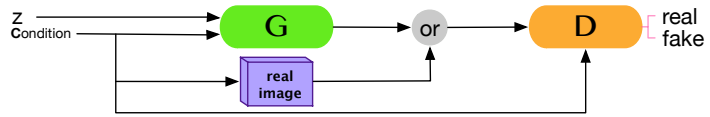


Figure 3: cGAN

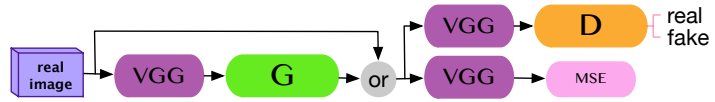


Figure 4: MGAN

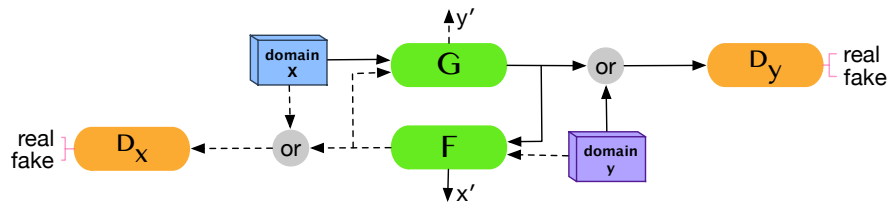


Figure 5: cycleGAN

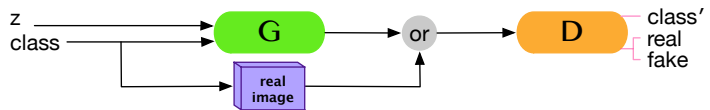


Figure 6: AC-GAN

Table 1: Metric explanation. (seg: segmentation, rec: reconstruction, det: detection, den: de-noising, reg: registration, and clas: classification) (TP: true positive, TN: true negative, FP: false positive, and FN: false negative)

Abbreviation	Metric	App	Abbreviation	Metric	Application
ROC	Receiver Operating Characteristic	seg	AUC	Area under the ROC Curve	seg, det
IoU	Intersection over Union: $\frac{\text{area of overlap}}{\text{area of union}}$	seg	Accuracy	$\frac{TP+TN}{TP+FP+FN+TN}$	seg, clas
Precision	$\frac{TP}{TP+FP}$	seg, clas	Specifity	$\frac{TN}{TN+FP}$	det
DSC	Dice similarity coefficient $\frac{TP}{2TP+FP+FN}$	seg, det, reg	Sensitivity	$\frac{TP}{TP+FN}$	seg, det
Recall	Sensitivity	seg, det, clas	F-score	$2 \frac{\text{Precision} \times \text{Recall}}{\text{Precision} + \text{Recall}}$	seg
ASD	age symmetric surface distance	seg	MSD	mean surface distance	seg
HSD	mean hausdorff surface distance	seg	OH	object hausdorff	seg
correlation of EF	correlation of ejection fraction	seg	MAE of Infarct size	mean absolute error on the surface of infarction (subjective)	seg
NCC	normalized cross correlation	det	correct detection		det
MSE	mean squared error	rec	NMSE	normalized MSE	rec
RMSE	root MSE	rec	NRMESE	normalized root MSE	rec
TRE	target registration error	rec	SIS	semantic interpretability score	seg
SNR	signal to noise ratio	rec	PSNR	peak SNR	rec, den
MOS	mean opinion score (subjective)	rec	GCF	global contrast factor	rec
SSIM	structural similarity	rec, den	Agatston score	clinical intensity weighted measure of calcified area	den
Noise suppression	scores in [1, 5](subjective)	den	Artifact reduction	scores in [1, 5](subjective)	den
Overall Quality	scores in [1, 5](subjective)	den	P2PE	point-to-point errors	den

simulation (Chuquicusma et al., 2018) and aids to gain deeper insights into the nature of data distributions and their latent structure.

Initial results have shown that the DCGAN can be used to synthesize realistically looking, small patches of prostate lesions (Kitchen and Seah, 2017), retinal images (Schlegl et al., 2017) or lung cancer nodules (Chuquicusma et al., 2018). The synthesized lung cancer nodules could even hardly be distinguished from real patches in a visual turing test involving two radiologists. Frid-Adar et al. (2018) make also use of the DCGAN, but for the synthesis of focal CT liver lesion patches from different classes. For each class, i.e. cysts, metastases and hemangiomas, they train a separate generative model. As the training dataset is originally quite small, they used heavily augmented data to train the GANs. In a set of experiments for liver lesion classification, the authors demonstrate that synthetic samples—in addition to data augmentation—can considerably improve a CNN classifier.

Bermudez et al. (2018) have shown that the DCGAN is also able to learn to mimic the distribution of entire MR data at considerably high resolution, even from a surprisingly small amount of samples. After training for 1500 epochs, the authors obtained visually compelling results which human observers could not reliably distinguish from real MR midline slices.

Baur et al. (2018b) compare the DCGAN, LAPGAN and some LAPGAN-modifications for skin lesion synthesis at high resolution. Due to the high vari-

ance within the training data, the small number of samples turned out not to be sufficient to train a reliable DCGAN. However the hierarchical LAPGAN and its variants showed promising synthesis results. The synthetic samples have also been successfully used in the training of a skin lesion classifier. Baur et al. (2018a) employed the recently proposed concept of progressive GAN growing (Karras et al., 2017) to synthesize high resolution images of skin lesions and showed stunning, highly realistic synthetic images which expert dermatologists could not reliably tell apart from real samples.

4.1.2. Conditional Image Synthesis:

CT from MR In many clinical settings, the acquisition of CT images is required. However, CT imaging puts the patient at the risk of cell damage and cancer because of radiation exposure. This motivates the synthesis of CT images from MR acquisitions. Nie et al. (2017) synthesize CT images from corresponding MR images with the help of a cascade of 3D Fully Convolutional Networks. In order to improve realism of the synthetic CT images they train the model with a pixel-wise reconstruction loss and an image gradient loss in addition to the adversarial training. The idea of utilizing a cascade of generators originates from the so-called Auto-Context Model (ACM). In ACMs a network provides its output as additional input to a succeeding network to provide context information and allow for refinements (Figure 7). While Nie et al. (2017) require corresponding pairs of CT and MR images for training, Wolterink et al. (2017a) successfully utilize cycleGANs to transform 2D MR images to CT images without the need for explicit, co-registered data pairs. Interestingly, their training led to even better results as the mapping is not affected by co-registration artifacts. Zhao et al. (2018a) use conditional GANs to map 3D MR data of the head to its CT counterpart to facilitate the segmentation of craniomaxillofacial bony structures. To obtain feasible image-to-image translation results, they propose so-called “deep supervision discrimination”, which—similarly to the perceptual loss—utilizes the feature representations of a pretrained VGG16 model to i) tell real and synthetic CT images apart and ii) provide gradient updates to the actual generator network.

MR from CT Similar to (Wolterink et al., 2017a), Chartsias et al. (2017) successfully leverage cycleGANs for unpaired image-to-image translation to generate pairs of cardiac MR image and its corresponding segmentation mask from pairs of cardiac CT slices and its ground-truth segmentation. The authors have shown that the performance of a segmentation model can be improved by 16% when the model is additionally trained with the synthetic data. They also showed that a model trained with only synthetic data performs only 5% worse than a model trained on real data. A major limitation of GANs, as pointed out by Cohen et al. (2018), is the lack of a guarantee that tumors/lesions are preserved during image-to-image translation. To cope with this issue, Jiang et al. (2018) propose a tumor-aware loss function for cycleGAN to synthesize MR images from CT images.

Retinal Image Synthesis Costa et al. (2017a) utilize a slight modification of the Pix2Pix framework (Isola et al., 2017) for the generation of high resolution

eye fundus image from binary images of vessel trees. In follow-up work Costa et al. (2017b) further introduce an adversarial autoencoder (AAE) which is trained to compress vessel tree images into a multivariate normal distribution and also consecutively reconstructing them. The resulting model synthesizes arbitrary high resolution vessel tree images by sampling from the multivariate normal distribution. The synthetic vessel tree images in turn can be fed into the image-to-image translation model, leading to an end-to-end framework for realistic, high resolution retinal image synthesis. Very similarly, Guibas et al. (2017) propose a two-stage approach, consisting of a GAN trained to synthesize vessel tree images from noise, and a Pix2Pix network (Isola et al., 2017) to generate realistic, high resolution pairs of groundtruth vessel segmentation and corresponding eye fundus image. In succession, the authors investigate the performance of a U-Net trained for segmentation using real data pairs and another model trained only on the synthetic samples, and find that training from only the synthetic data leads to a slightly inferior model.

Zhao et al. (2017) also leverage the Pix2Pix framework for synthesizing filamentary structured images, i.e. eye fundus images and neurons from binary segmentation masks. In comparison to Costa et al. (2017a,b), the authors also provide their framework with a reference image for style. To enable style transfer, they train the generator with the feedback of a VGG-network in addition to the discriminator. Opposed to Pix2Pix, they do not introduce noise with the help of dropout, but by augmenting noise to the bottleneck of the encoder-decoder network.

PET from CT PET images are frequently used for diagnosis and staging in oncology. The combined acquisition of PET and anatomical CT images is a standard procedure in clinical routine. Furthermore, PET/CT imaging is becoming an important evaluation tool for new drug therapies. However, PET devices are expensive and involve radioactivity, thus put patients at risk. Consequently, the medical imaging analysis community has been working on synthesizing PET images directly from CT data. Initial promising results to synthesize liver PET images from CT data with a conditional GAN have been obtained by Ben-Cohen et al. (2017). The cGAN, inspired by Isola et al. (2017), is able to synthesize very realistic looking PET images. However, its performance has low response to underrepresented tumor regions, which leads to poor tumor detection performance in a set of use-case experiments. In comparison, an FCN for PET image synthesis is capable of synthesizing tumors, but produces blurry images in general. By blending corresponding synthetic PET images coming from the conditional GAN and the FCN, they are able to achieve very high tumor detection performance. Similarly, Bi et al. (2017) utilize a cGAN for synthesizing high-resolution PET images from pairs of CT images and binary labelmaps. While CT images alone would be sufficient as input, the authors emphasize that adding a labelmap leads to globally more realistic, synthetic output. Because of the two-channel input to the generator, they refer to their network as the multi-channel GAN. Further, the authors validated their synthetic PET images with a tumor detection model trained on synthetic data and obtained comparable results to a model trained with real data. They show that

synthetic data can be beneficial when labeled data is scarce.

PET from MRI Measuring the myelin content in PET images of the human brain is valuable for monitoring disease progression, understanding pathophysiology and evaluating treatment efficacy of Multiple Sclerosis (MS). Unfortunately, PET imaging for MS is costly and invasive as it requires the injection of a radioactive tracer. Wei et al. (2018) successfully utilize a cascade of two conditional GANs, based on 3D U-Nets for the generators and 3D CNNs for the discriminators, to synthesize PET images from a set of different MR volumes. The authors noted that a single cGAN was insufficient for the task at hand as it produced blurry images. Splitting the synthesis task into smaller, more stable subproblems seemed to drastically improve the results.

Ultrasound Hu et al. (2017) propose a cGAN conditioned on 3D voxel locations for synthesizing 2D freehand Ultrasound (US) images of a fetus phantom. In comparison to the standard cGAN, the authors find it necessary to transform the pixel locations into featuremaps and inject these at various layers of the generator to facilitate training. In their experiments, they demonstrate the capability of simulating US images at locations which are unseen to the network. Further, they quantify the generation of sound images by comparing the location of clinically relevant anatomical landmarks in synthetic and real images, and verify the realism of the generated images in a usability study.

Tom and Sheet (2018) apply GANs for intravascular US (IVUS) simulation in a multi-stage setup. A first generator, conditioned on physically simulated tissue maps, produces speckle images. The second generator maps the speckle images to low resolution, synthetic 64×64 pixels sized US images. A third generator transforms these low resolution images into high resolution samples at a resolution of 256×256 pixels. In a visual turing test, the synthetic images could not reliably be distinguished from real ones.

X-ray Mahapatra et al. (2018) train a cGAN for chest X-ray synthesis from perturbed segmentation maps and combine it with Bayesian Neural Networks for Active Learning.

Stain Normalization Conditional GANs have also been leveraged for coping with the variance in digital histopathology staining, which is well known to cause problems for CAD systems. Cho et al. (2017) point out that tumor classifiers do not only generalize poorly across data with different stains, but also that existing stain-normalization approaches fail to preserve important image features. To overcome this issue, they propose a feature-preserving cGAN for stain style transfer. First, they map histopathology images to a canonical gray-scale representation. In succession, they leverage a cGAN to transform these gray-scale images into RGB images with the desired staining. The benefits of employing an additional feature-preserving loss on the hidden layers of the discriminator are experimentally validated by obtaining the smallest performance degradation among a variety of State-of-the-Art (SOTA) stain transfer methods.

Bayramoglu et al. (2017) leverage the Pix2Pix framework for virtual H&E staining on unstained hyperspectral microscopy patches. The authors report promising quantitative results, but also point out to require expert feedback in

order to draw a valid conclusion.

Bentaieb and Hamarneh (2018) try to tackle the stain transfer problem with the help of an AC-GAN by simultaneously training a conditional GAN for stain-transfer and a task-specific network (i.e. a segmentation or classification model). The joint optimization of the generator, the discriminator and the task-specific network drives the generator to produce images with relevant features being preserved for the task-specific model.

Aformentioned methods rely on paired training data to map from a source to target staining. Such a dataset is often hardly available and requires pre-processing such as co-registration. Moreover, co-registration itself is not perfect and is prone to produce artifacts. Shaban et al. (2018) alleviate the need for paired training data and co-registration by employing cycleGANs for the task of stain transfer. In a broad set of experiments on different datasets, they obtain visually more compelling stain transfer results than previous deep-learning and non-deep learning based methods.

Microscopy Han and Yin (2017) propose a framework similar to Pix2Pix for transferring Phase Contrast (PC) and Differential Interference Contrast (DIC) in microscopy images to one another. A U-net like generator is trained to synthesize the image of a certain modality from a source modality and the corresponding cell mask. Interestingly, two discriminators are employed to differentiate between i) pairs of (real source, real target) versus (real source, synthesized target), and ii) pairs of (cell mask real source) versus (cell mask, synthesized target). In a set of qualitative and quantitative evaluations they rank their two-discriminator approach against the single-discriminator Pix2Pix framework. They report improved quantitative results when transferring from DIC image to Phase Contrast, and comparable results when trying to map from Phase Contrast to DIC. The authors amount the comparable performance of the latter to the details already present in PC images, which leaves the cell mask with very little impact on the synthesis outcome.

Blood Vessels Machine Learning driven analysis methods for detecting atherosclerotic plaque or stenosis in coronary CT angiography (CCTA) are powerful, but data-hungry. To deal with the lack of labeled data, Wolterink et al. (2018) propose to synthesize plausible 3D blood vessel shapes with the help of a WGAN fed with noise and attribute vectors. To facilitate the synthesis in 3D at appropriately high resolution, the authors generate 1D parameterizations of primitives which characterize blood vessels as a proxy for the final vessel rendering. Alternatively to CT, Magnetic Resonance Angiography (MRA) has evolved as an important tool for visualizing vascular structures. However, often it is not acquired alongside the standard protocols. Olut et al. (2018) propose the so-called steerable GAN to synthesize MRA images from T1 and T2-weighted MR scans, potentially alleviating the need for additional MR scans. Their conditional, steerable GAN combines a ResNet-like generator with a PatchGAN-discriminator. Also they propose an ℓ_1 -loss between real and synthesized image as well as a steerable filter loss to promote faithful reconstructions of vascular structures.

The unconditional methods are summarized in Table 2, whereas the condi-

tional GAN variants are summarized in Table 3 and 4. In particular, we report the method, containing the underlying GAN architecture, the image modalities on which the particular method operates, the datasets which have been used and the resolution of the synthesized images. We further mark whether a paper has been peer-reviewed or not. Since losses are a substantial part of the underlying GAN framework, we do not explicitly report them here. Further, we do not report any quantitative results since they i) are in many case unavailable, ii) hardly interpretable and iii) overall hardly comparable.

In general, many interesting GAN-based approaches have been proposed for both unconditional and conditional image synthesis. However, often the validity of the method at hand is questionable and requires more elaboration. For instance, in many visual turing tests it seemed to have been fairly easy to distinguish between real and generated images (Frid-Adar et al., 2018; Chuquicusma et al., 2018; Hu et al., 2017) due to artifacts in synthetic samples. Hu et al. (2017) and Chuquicusma et al. (2018) tackle this problem by applying anisotropic or gaussian filtering to both real and fake samples before presenting them to the raters (Hu et al., 2017; Chuquicusma et al., 2018). This is only valid as long as blurry images still contain the required amount of information for the task at hand. Another problem of GAN is mode collapse, resulting in very similar looking synthetic samples. Particularly in the works of Kitchen and Seah (2017) and Schlegl et al. (2017), where samples look fairly similar, it should be considered if mode collapse has occurred. In general, the community still lacks a meaningful, universal quantitative measure for judging realism of synthetic images. Regardless of the realism, aforementioned works have shown that GANs can be used successfully for data simulation and augmentation in classification and segmentation tasks. How exactly realism, artifacts and other specific properties of generated samples affect a machine learning model generally remains an open question.

Table 2: Unconditional GANs for Medical Image Synthesis

Method	Architecture	Modality	Dataset	Resolution	PR	Code
Kitchen and Seah (2017)	DCGAN	MRI Prostate Lesions	SPIE ProstateX Challenge 2016 (330 MRI Scans)	16×16	No	No
Chuquicusma et al. (2018)	DCGAN	CT Lung Cancer Nodules	LIDC-IDRI (1145 nodules)	56×56	Yes	No
Frid-Adar et al. (2018)	DCGAN	focal CT liver lesion patches	non-public (182 CT scans)	64×64	Yes	No
Bermudez et al. (2018)	DCGAN	2D axial brain MR slices	Baltimore Longitudinal Study of Aging (BLSA) (528 healthy subjects)	220×172	Yes	No
Baur et al. (2018b,a)	DCGAN, LAPGAN, PGAN	Skin Lesions (Dermoscopy)	ISIC2017 (2000 samples) ISIC2018 (10,000 samples)	256×256	No	No

4.2. Segmentation

Segmentation of objects and organs in medical images is an essential prerequisite for many applications such as detection, classification, and shape analysis. The tedious and time-consuming nature of manual segmentation made automatic methods the most active field of Deep-Learning research in medical

Table 3: Conditional GANs for Medical Image Synthesis

Method	Architecture	Modality	Dataset	Resolution	PR	Code
Nie et al. (2017)	3D Autocontext FCN with adversarial loss, image gradient loss and ℓ_2 -loss	MR to CT	ADNI (16 subjects) and 22 non-public pelvic image pairs	$32 \times 32 \times 32$ (MRI) to $16 \times 16 \times 16$ (CT)	Yes	Yes
Wolterink et al. (2017a)	cycleGAN	2D sagittal brain MR and CT slices	non-public (24 subjects)	256×256	No	No
Zhao et al. (2018a)	3D cond. GAN	MR to CT	ADNI (16 subjects)	$152 \times 184 \times 149$	Yes	No
Chartsias et al. (2017)	cycleGAN	2D cardiac MR w. segmentation mask to cardiac CT w. segmentation mask	non-public (20 CT/CTA and 20 MRI)	232×232	No	No
Jiang et al. (2018)	Tumor-Aware cycleGAN	CT to MR	NSCLC (The Cancer Imaging Archive, 377 scans) & non-public (42 scans)	256×256	Yes	No
Costa et al. (2017a,b)	AAE and Pix2Pix	2D binary vessel tree images to retinal images	DRIVE (40 samples) MESSIDOR (1200 samples)	512×512	Yes	Yes
Jin et al. (2018)	3D cond. GAN	CT (lung nodules)	LIDC (1018 scans)	$64 \times 64 \times 64$	Yes	No
Guibas et al. (2017)	GAN and Pix2Pix	2D binary vessel tree, images to retinal	DRIVE (40 samples) MESSIDOR (1200 samples)	512×512	No	Yes
Zhao et al. (2017)	Pix2Pix w. Style Transfer	eye fundus, microscopic neuronal	DRIVE (40 samples) STARE (20 samples) HRF (45 samples) NeuB1 (112 samples)	512×512 and higher	No	Yes
Ben-Cohen et al. (2017)	Pix2Pix and FCN	2D liver tumor CT to PET	non-public (25 pairs)	n/a	No	No

image analysis (Litjens et al., 2017). However, the pixel-wise based evaluation and optimization procedure in deep networks is not sufficient to extract notions of anatomical structures. This drawback requires additional corrections on top of CNNs such as Conditional Random Fields (CRFs) and Statistical Shape Models (SSMs), which are not easily optimizable (Chen et al., 2018b; Tack et al., 2018). GANs, providing a different learning flow, are a potential solution to address this problem. In the following Subsection we focus on GAN-based segmentation approaches, categorized based on specific parts of the anatomy.

4.2.1. Brain:

The proposed methods for brain structures and abnormality segmentation comprise both supervised and unsupervised methods. Moeskops et al. (2017) demonstrate that using the GAN training strategy in CNNs enhances not only the performance of semantic segmentation methods but also brings the performance of non-semantic segmentation methods closer to semantic ones. Li et al. (2017a) highlight the superior performance of GANs in the segmentation of normalized/equalized patches of brain tumors. Xue et al. (2018) propose the SegAN framework which employs the U-Net as the generator architecture of GAN. They show that pixel-dependencies are learned better by using a multi-scale loss function in addition to adversarial and pixel-wise losses. One of the known challenges with most of supervised segmentation methods is the performance degradation on unseen images. Kamnitsas et al. (2017) propose to leverage an adversarial framework to address this problem for unsupervised

Table 4: Conditional GANs for Medical Image Synthesis

Method	Architecture	Modality	Dataset	Resolution	PR	Code
Bi et al. (2017)	cond. multi-channel GAN	CT and segmentation pairs to PET images	non-public (50 subjects)	200×200	No	No
Hu et al. (2017)	spatially cond. GAN	2D US	non-public fetus phantom (26,396 images)	160×120	No	Yes
Tom and Sheet (2018)	multi-stage cond. GAN	simulated tissue maps to 2D Intravascular US	IVUS challenge (2,175 images)	256×256	Yes	No
Mahapatra et al. (2018)	cond. GAN	Segmentation maps to synthetic X-ray images	SCR chest XRay database (247 images) NIH (400 images)	512×512	Yes	No
Cho et al. (2017)	feature-preserving cond. style-transfer GAN	Digital Histopathology	CAMELYON16 (400 slides)	n/a	No	No
Bayramoglu et al. (2017)	Pix2Pix	Hyperspectral microscopic to H&E stained	non-public (2838 image pairs)	64×64	No	Yes
Bentaieb and Hamarneh (2018)	ACGAN	Digital Histopathology	MITOS-ATYPPIA14 (11 slides) MICCAI16 GlaS challenge (165 slides) non-public ovarian carcinoma (135 slides)	250×250	Yes	No
Shaban et al. (2018)	cycleGAN	Digital Histopathology	MITOS-ATYPPIA14 (11 slides) Camelyon16 (400 slides)	256×256	Yes	Yes
Han and Yin (2017)	cond. GAN with two Discriminators	DIC & Phase Contrast Microscopy	non-public (1,600 pairs)	256×256	No	No
Wolterink et al. (2018)	WassersteinGAN	Geometric parameters extracted from CCTA	non-public (4,412 centerlines)	n/a	No	No
Olut et al. (2018)	cond. steerable GAN	MRA from T1 & T2w MRI axial slices	IXI Dataset (578 pairs)	n/a	No	No

domain adaptation in brain lesion segmentation. In this method, a domain discriminator network is employed to make the segmentation network invariant to input from different domains. The varying appearance of anatomical tissues in multi-modal images leads to improved segmentation performance. For the segmentation of bony structures in brain images Zhao et al. (2018b) propose to synthesize CT images from MRI images using GANs and then use both of them as the input to a segmentation network. They proposed a segmentation architecture called Deep-supGAN which is optimized with 5 different losses: an adversarial loss, a voxel-wise loss, and 3 perceptual losses defined on differences between VGG extracted features. For multi-class classification of brain tumors, Rezaei et al. (2017) propose a method combining the cGAN and MGAN, where class labels define conditions.

4.2.2. Chest:

Bad quality, local artifacts and the overlap of lung and heart area are the main obstacles for segmentation of chest X-Ray images. As existing approaches in this field do not provide consistency between global and local features, Dai et al. (2018) propose the SCAN architecture, achieving human levels of performance in heart/lung segmentation. In this method, the generator is pre-trained with a pixel-wise loss function to address the instability problem of GANs.

4.2.3. Eye:

Many CNN-based approaches perform even better than human experts in retinal vessel segmentation. However, blurriness and false positive segmentations near minuscule or faint branches constitute a problem which is not solved yet. Son et al. (2017); Lahiri et al. (2017) propose GANs as a solution to this problem. For optic disc and cup segmentation in 2D color fundus images, Shankaranarayana et al. (2017) successfully leverage a cGAN.

4.2.4. Abdomen:

Yang et al. (2017a) propose GANs which employ the U-Net as the generator to segment liver in 3D CT images of the abdomen. Kim and Ye (2018) propose to use the cycleGAN for both liver and liver tumor segmentation. To address the problem of miss-segmentation of tiny tumors, they propose a new architecture based on the U-Net (polyphase U-Net) for the generator. Spleen segmentation in MRI images is a challenging task due to the varying size and shape of this organ. To address this problem Huo et al. (2018) propose a cGAN combined with the global convolutional network (GCN) (Peng et al., 2017) as the generator architecture. They showed that larger convolutional kernels in the GCN in addition to adversarial training enhances the segmentation performance on objects with large variability.

4.2.5. Microscopic images:

Automatic segmentation of microscopic images is challenging due to the variety of size, shape, and texture. (Sadanandan et al., 2017; Arbelle and Riklin-Raviv, 2018). Sadanandan et al. (2017) propose to use GANs with special training loss function, which considers a weight to specify which pixels in foreground/background are more important. Arbelle and Riklin-Raviv (2018) use GANs with special blocks (convolution followed by batch normalization) in the discriminator for the same problem. Zhang et al. (2017b) propose DAN – a combination of DCAN (Chen et al., 2016) and VGG16 – which is trained with both supervised and unsupervised strategies to provide high-quality segmentation masks for unseen images.

4.2.6. Cardiology:

Low contrast, high level of noise, and cardiac motion are challenges for segmenting cardiology images. To segment the Left Ventricle (LV) in low-contrast cardiology images, Dong et al. (2018) propose the VoxelAtlasGAN which employs a V-Net (Milletari et al., 2016) atlas-based segmentation in the generator of a cGAN framework (Figure 8). Also, Xu et al. (2018) propose to benefit from the cGAN on top of atlas-based segmentation to facilitate feature extraction of all time sequences frames for precise segmentation of myocardial infarction. Since in segmentation, residual (non-RoI) information in addition to RoI features can make segmentation results more realistic, Chartsias et al. (2018) and Thomas Joyce (2018) propose a reconstruction strategy based on both of these features. They added a reconstruction loss to the optimization procedure of

GAN as a controlling parameter. For semi-supervised and unsupervised segmentation, Chatsias et al. (2018) and Thomas Joyce (2018) propose to use the cycleGAN and LSGAN architectures, respectively. They also proposed some loss functions to address over-segmentation in large regions with varying intensity.

4.2.7. *Spine:*

In medical image analysis of the spine, machine learning based approaches suffer from not properly learning the anatomy of the discs in vertebrae for segmentation and localization. Sekuboyina et al. (2018) propose a butterfly shape GAN model to segment disc regions in two views of vertebrae.

Tables 5 to 11 summarizes GAN-based segmentation methods. These mainly use GAN/cGAN/DCGAN in addition to pixel/voxel-wise optimization loss functions. Also, CycleGAN and reconstruction loss strategies are proposed to consider non-RoI features for more precise segmentation. In the reviewed methods, U-Net and ResNet - due to providing general identification features - are the most popular segmentation networks for the generator architecture. However, in the reviewed papers, some limitations exist which trouble a clear judgment on the proposed methods. The ability of GANs to consider both global and local information performs close to semantic segmentation, even though difficulties related to semantic methods, unsupervised learning, and detail preservation are addressed. Tables show that GAN-based methods are trainable using a varying amount of data from 10 to 1000+ input samples. However, there are some limitations in the information provided in the reviewed papers. Some papers only used the DICE similarity score for evaluation, which its practical meaning is debatable.

Experimental results generally show that the competition between segmentors using and not using adversarial training is tightly closed. However in microscopic images segmentation, GANs made a significant enhancement.

4.3. *Reconstruction*

Fast MR reconstruction without sacrificing details is a core problem in medical imaging. Fast acquisition and reconstruction directly reduces any kind of motion artifacts and is thus highly desirable.

Classic compressed sensing-based solutions directly use k-space information to reconstruct images (Yu et al., 2017). The ability to promote realism in images with fast inference makes GANs an obvious candidate for solving the MR reconstruction problem. GAN-based MR reconstruction research has a major focus on modifying well-known architectures and combining them with appropriate loss functions.

4.3.1. *DAGAN-based strategies*

Early research on GAN-based MR reconstruction focuses on the DAGAN architecture (Yang et al., 2017b). In this method, a perceptual loss is added to adversarial and pixel-wise losses to compare deep extracted features in real and

Table 5: Segmentation GAN-based methods - Brain

method	Arch	loss	modality	dataset	performance	PR	code
Moeskops et al. (2017)	GAN	Adv, cross entropy	MRI	MICCAI 2012 Challenge Train:15	DSC = 0.92±0.03	Yes	No
				MRBrainS13 challenge Train:5 Test:15	DSC = 0.85±0.01		
Li et al. (2017a)	GAN	Adv	MRI	BRATS 2017 Train:285	(Whole, Core, Enhancing) DSC = 0.87, 0.72, 0.68 sensitivity = 0.87, 0.72, 0.68	Yes	No
Xue et al. (2018) SeGAN	U-Net, GAN	Adv, multiScale	MRI	BRATS 2013 Train:25	(whole, Core, Enhanced) DSC = 0.84, 0.70, 0.65 Precision = 0.87, 0.80, 0.68 Sensitivity = 0.83, 0.74, 0.72	Yes	No
				BRATS 2015 Train:274	DSC = 0.85, 0.70, 0.66 Precision = 0.92, 0.80, 0.69 Sensitivity = 0.80, 0.65, 0.62		
Kamnitsas et al. (2017)	GAN, 3D-CNN	Adv, SGD	MRI (TBI)	unknown Train:61	DSC = 0.62 Recall = 0.58 Precision = 0.71	Yes	Yes
Zhao et al. (2018b) Deep-supGAN	GAN, VGG16	Adv, Preceptual, voxel-wise	MRI 3D	ADNI Train:16	DSC = 94.46	Yes	No
Rezaei et al. (2017)	c-GAN, MGAN	Adv	MRI	BRATS 2017 Train:285	(Whole, core, Enhanced) DSC = 0.70, 0.55, 0.40 Sensitivity = 0.68, 0.52, 0.99 Specificity = 0.99, 0.99, 0.99	Yes	No

Table 6: Segmentation GAN-based methods - Chest

method	Arch	loss	modality	dataset	performance	PR	code
Dai et al. (2018) SCAN	VGG, ResNet, GAN	multi-class, cross-entropy, Adv	X-Ray	JSRT Montgomery Train:382	(Lungs, Heart) DSC = 0.973, 0.927 IoU = 0.947, 0.866	Yes	No

Table 7: Segmentation GAN-based methods - eye

method	Arch	loss	modality	dataset	performance	PR	code
Son et al. (2017)	U-Net, GAN	Adv, Cross entropy	Funduscopy (Retina)	DERIVE Train:20	DSC = 0.829 ROC = 0.9803 precision = 0.9149	No	Yes
				STARE Train:10 Test:10	DSC = 0.834 ROC = 0.9838 precision = 0.9167		
Lahiri et al. (2017)	DCGAN	Adv	Funduscopy (Retina)	DERIVE (blood vessels) Train:20 Test:20	AUC = 0.945	Yes	No
Shankaranarayana et al. (2017)	c-GAN, ResU-net	Adv, L1	Funduscopy (Retina)	RIM-ONE Train:159	(disc, cup) F-score = 0.97, 0.94 IOU = 0.89, 0.76	Yes	No

Table 8: Segmentation GAN-based methods - Abdominal

method	Arch	loss	modality	dataset	performance	PR	code
Yang et al. (2017a)	U-Net, auto-encoder	Adv, cross-entropy	CT 3D (Liver)	unknown, MICCAI (SLiver07) Train:1000+	DSC = 0.95 ASD = 1.90	Yes	No
Kim and Ye (2018)	U-Net, cycleGAN	cycleGAN, Cross entropy, L2	CT 3D (Liver)	LiTS2017 Train:73 Test:9	(liver, lesion) DSC = 0.89, 0.46 Recall = 0.94, 0.5 Precision = 0.86, 0.48	Yes	No
Huo et al. (2018) SSNet	GCN, cGAN	Adv, DSC	MRI	unknown Train:45 Test:15	DSC = 0.9260	Yes	No

generated information, which also enhances the stability of the model. A series of work refines the DAGAN architecture over time (Yu et al., 2017; Yang et al.,

Table 9: Segmentation GAN-based methods - Microscopic

method	Arch	loss	modality	dataset	performance	PR	code
Sadanandan et al. (2017)	GAN, U-net, Res-Net, MS CNN	Adv, weighted loss	Cell 2D	unknown Train:5 × 6000	F-score = 0.70 Precision = 0.74 Recall = 0.69	Yes	No
Arbelle and Riklin-Raviv (2018)	GAN (rib cage)	Adv	Cell 2D	H1299 Train:2 - 11	F-score = 0.89 Precision = 0.82 Recall = 0.85	Yes	Yes
Zhang et al. (2017b) DAN	GAN, DCAN, VGG	Adv, Multi-scale cross entropy	Fungus 3D	2015 MICCAI Gland Challenge Train:85 Test:20	F-score = 0.88 DSC = 0.865 OH = 74.55	Yes	No

Table 10: Segmentation GAN-based methods - Cardiology

method	Arch	loss	modality	dataset	performance	PR	code
Dong et al. (2018) VoxelAtlasGAN	cGAN, V-Net	Adv, intensity, label	Echo 3D	unknown Train:25 Test:35	DSC = 0.95 MSD = 1.85 HSD = 7.26 corr-of-EF = 0.91 time = 0.1	Yes	No
Xu et al. (2018) MuTGAN	GAN, ConvLSTM, 3DConv	Adv, MAE, DSC	3T MR Cardiac cine, DE-MR	unknown Train:140 Test:	DSC=0.90 Accuracy=96.46 Infarct size=22.3	Yes	No
Chartsias et al. (2018)	cycleGAN	Adv, DSC, MAE	Cine MR 3D	2017 ACDC Challenge, Edinburgh Imaging Facility QMRI Train:128 Test:50	F-score = 0.771	Yes	Yes
Thomas Joyce (2018) DAN	LSGAN, U-net	Adv, Intensity-Var, Over-Seg penalty, Recons	CT or MR Cardiac 2D	2017 MM-WHS Challenge Train:20 Test:3MR, 3CT	(MR) DSC = 0.66 (CT) DSC=0.5	Yes	No

Table 11: Segmentation GAN-based methods - Spine

method	Arch	loss	modality	dataset	performance	PR	code
Sekuboyina et al. (2018) Btrfly Net	GAN, Btrfly-Net	Adv, Btrfly-Net	CT 3D	Glocker et al. (2013) Train:242 Test:60	Precision=0.84 Recall=0.83 F1-score= 0.84	Yes	No

2017b) by manipulating loss functions to preserve frequency information(Figure 9). A combined loss function is defined as:

$$L_G = \alpha L_{image-MSE} + \beta L_{freq-MSE} + \gamma L_{VGG} + L_{GAN} \quad (6)$$

The next update of DAGAN is introduced by Seitzer et al. (2018) who propose to add a refinement network (Figure 10) to separate pixel-wise and perceptual information-based training.

A similar architecture (Figure 10) is proposed by Quan et al. (2017), where the authors consider a cyclic training strategy based on the reconstruction of data in the lost frequencies. Moreover, they propose to use a chain of generators to address the ambiguities made in earlier generators.

4.3.2. 3D super-resolution strategies

Sánchez and Vilaplana (2018) adapt the SRGAN (Ledig et al., 2017a) with 3D convolutional layers to deal with volumetric information and enhance the

stability of the proposed GAN model. Their loss function combines a pixel-wise loss with a Gradient-Based Loss (GDL) (Mathieu et al., 2015) to address the blurring effect in the reconstructions. Li et al. (2017b) propose a 3DSRGAN along with two loss functions to control data interpolation and prevent over-fitting. In addition to the adversarial and the MSE losses, two other objectives are defined to overcome over-fitting and control data interpolation. The considerable memory footprint of 3D convolutions is a well-known challenge. To address this problem, Chen et al. (2018c) propose a multi-level Densely Connected Super-Resolution Network (mDCSRN), which is a combination of the WGAN model (Arjovsky et al., 2017) and a modified version of DenseNet (Chen et al., 2018a).

4.3.3. Other Methods

Other GAN-based reconstruction methods mostly introduce additional loss functions to the original framework. In (Mardani et al., 2017) and (Shitrit and Riklin-Raviv, 2017) pixel-wise losses, in (Zhang et al., 2018) and (Han and Yin, 2018) perceptual losses, in (Mahapatra et al., 2017) a saliency loss, and in (Ravi et al., 2018) Voronoi-vectorization and regularization losses are proposed to be added to the adversarial loss. Mardani et al. (2017) proposes to use the LSGAN as a solution to address training instability.

Table 12, 13 and 14 summarizes properties of mentioned methods and their performance. While many architectural modifications of the GAN are proposed, it seems that ResNet is the most popular architecture for the generator. All the methods introduce a pixel-wise loss in addition to the adversarial loss. Also, other loss functions are introduced to preserve essential information in the lost data reconstruction. Due to their synthesis abilities, GANs can provide good performance in the reconstruction of lost data in medical images. Textural features are essential for diagnosis, and GANs should be trained with additional loss functions to satisfy these aspects. Generally, results of reviewed papers show that GANs in comparison with other methods perform faster and more accurate in data reconstruction. Most of the methods need a huge amount of data to provide the convergence through all loss functions defined. Moreover, evaluation metrics are not necessarily comprehensive to explore the preservation of identical features in the results.

4.4. Detection

The detection of anomalies from images with supervised Deep Learning algorithms requires a large amount of annotated training data. GANs tackle this problem in a different ways: i) by enhancing datasets with synthetic samples, or ii) by modeling distributions from which anomalies can be detected as outliers.

For aggressive prostate cancer detection (Kohl et al., 2017) and skin lesion detection (Udrea and Mitra, 2017) propose to use the U-Net architecture as the generator of a GAN and a cGAN, respectively. In prostate US, the low contrast of tumor boundaries challenges contour detection. (Tuysuzoglu et al., 2018) address this problem using GANs.

Table 12: Reconstruction GAN-based methods - DAGAN based

method	Arch	loss	modality	dataset	performance	PR	code
Yu et al. (2017)	cGAN, U-Net	Adv, Pix-wise, Perceptual, Refinement	MRI	IXI, MICCAI Grand Challenge 2013 Train:1605+100 Test:50	mask 30%: NMSE=0.09±0.02 PSNR=39.53±4.12 (CPU, GPU) time=0.2±0.1, 5.4±0.1(ms)	No	No
Yang et al. (2017b) DAGAN	cGAN, U-Net	Adv, Pix-wise, Frequency, Perceptual, Refinement	MRI	MICCAI Grand Challenge 2013 Train:21128 Test:9854	mask 30%: NMSE=0.08±0.02 PSNR=40.20±4.07 (CPU, GPU) time= 0.2±0.1, 5.4±0.1(ms)	Yes	No
Seitzer et al. (2018)	cGAN, U-Net	Adv, feature matching, Perceptual, penalty	MRI Cardic	unknown Train:3000 3D Test:1200	PSNR=31.82±2.28 MOS=3.24±0.63 (max=3.78±0.45) SIS=0.94 (max=1)	Yes	No
Quan et al. (2017) RefineGAN	GAN chain, ResNet	Adv, Cyclic	MRI	Brain: IXI Train:100 Test:100 Chest: Data Science Bowl challenge Train:100 Test:100	mask 30%, time:0.16(s) SSIM=0.97±0.01 PSNR=38.71±2.57 mask 30%, time:0.18(s) SSIM=0.97±0.01 PSNR=38.64±2.76	No	Yes

Table 13: Reconstruction GAN-based methods - 3D super-resolution

method	Arch	loss	modality	dataset	performance	PR	code
Sánchez and Vilaplana (2018)	SRGAN, subpixel-NN	LSGAN, GDL, Pixel-wise	MRI (Brain)	ADNI database Train:470 Test:119	(Scale 2, Scale 4) PSNR=39.28, 33.58 SSIM=0.98, 0.95	Yes	No
Li et al. (2017b)	ResNet, GAN	Adv, Pixel-wise 3D variation	MRI (Brain)	Glioma Patients Train:30+10	PSNR=24.2 MSE=262.2	Yes	No
Chen et al. (2018c) mDCSRN	DenseNet, WGAN	MSE, WGAN	MRI (Brain)	unknown Train:891 Test:111	PSNR=35.88 SSIM=0.94 NRMSE=0.0852	Yes	No

Table 14: Reconstruction GAN-based methods - other

method	Arch	loss	modality	dataset	performance	PR	code
Mardani et al. (2017) GANCS	ResNet, LSGAN	Adv	MRI (Chest)	contrast-enhanced MRI abdomen pediatric patients Train:300 Test:50	SNR=20.48 SSIM=0.87 Time=0.02	No	No
Shitrit and Riklin-Raviv (2017)	ResNet, GAN	Adv	MRI (Brain)	unknown Train:1560 Test:346	PSNR=37.95	No	No
Zhang et al. (2018) GANCS	ResNet, GAN, VGG	Adv	MRI (Brain 2D)	unknown Train:170 Test:43	PSNR=32.32 SSIM=0.88 Time=0.37	Yes	No
Mahapatra et al. (2017)	ResNet, GAN	Adv, CNN saliency	Retinal	unknown Funduscopy(5000 data))	(Scale 4, Scale 8) SSIM=0.89, 0.84 RMSE=6.2, 7.5 PSNR=44.3, 39db	Yes	No
Han and Yin (2018)	Su et al. (2013), GAN	Adv, Perceptual	Microscopy (Cell)	unknown Train:11000 Test:500	PSNR = 27.8591	Yes	No
Ravi et al. (2018)	Ledig et al. (2017b), GAN, Cyclic	Adv, Regular	Endo- microscopy	André et al. (2011) Train:202 Test:36	SSIM=0.8.7 $\Delta GCF_{\overline{HR}}=0.66$ $\Delta GCF_{\overline{LR}}=0.37$ $Tot_{CS}=0.66$	Yes	No

A different approach towards unsupervised anomaly detection is to model the distribution of normal data with GANs. Then the GAN reconstructs the most similar normal image to the query image and anomalies can be detected

as discrepancies between the query and the reconstructed image.

Schlegl et al. (2017), introducing an unsupervised framework –named AnoGAN, showed that such an idea can be effective in detecting anomalies in OCT images of the retina. Succeeding work in (Chen and Konukoglu, 2018) and (Baur et al., 2018c) modified this framework for anomaly detection in brain MR images. Inspired by the AnoGAN, Baumgartner et al. (2018) propose the Visual Attribution GAN (VA-GAN) for Alzheimer’s disease detection. This model extracts the map of changes that convert the class of the image from healthy to diseased and use it for abnormality detection. CNNs (Shwartz-Ziv and Tishby, 2017) show good performance in detecting high contrast lesions arising from Alzheimer’s, but the VA-GAN also detects low contrast lesions.

Table 15 summarizes these papers. Papers proposed in anomaly detection by GANs have more structural complexity in comparison to previous applications because they benefit from different aspects of GANs. In fact, the role of the discriminator is highlighted in detection methods. The aforementioned methods show good performance in anomaly detection while they reduce the number of training data significantly. However, varying datasets and metrics employed for the experiments challenge a fair comparison between the methods.

Table 15: Detection GAN-based methods in medical image processing.

method	Arch	loss	modality	dataset	performance	PR	code
Kohl et al. (2017)	U-Net, GAN	MSE, GAN	MRI (prostate)	Heidelberg Train:188	Specificity=0.98±0.14 DSC=0.41±0.28 Sensitivity=0.55±0.36	No	No
Udrea and Mitra (2017)	cGAN, U-net	-	Natural Skin	unknown Train:2417 Test:583	(Subjective) Correct Detect = 0.914	Yes	No
Tuysuzoglu et al. (2018)	GAN	Adv, Local, Contour	Ultra-Sound (prostate)	unknown Train:4570 Test:229	DSC = 0.92±0.3	Yes	No
Schlegl et al. (2017) AnoGAN	DCGAN	Adv	SD-OCT scans	unknown Train:270 Test:20	Precision= 0.8834 Recall= 0.7277 Sensitivity=0.7279 Specificity=0.8928 AUC=0.89	Yes	No
Chen and Konukoglu (2018)	AnoGAN, WGAN-GP	WGAN-GP, Regular	MRI (brain)	BRATS Train:35 Test:42	AUC = 0.92	No	No
Baumgartner et al. (2018) VA-GAN	WGAN, U-Net	Adv	MRI (brain)	ADNI Train:80 Test:20	NCC = 0.27	Yes	Yes

4.5. De-noising

Imaging in diagnostic radiology typically involves a trade-off between image contrast and radiation hazard. A higher contrast might lead to better diagnosis, but exposes the patient to unwanted excessive radiation, whereas reduced radiation exposure leads to lower contrast and lower Signal-to-Noise Ratios. Deep Learning has been successfully used to denoise low-contrast images and to enhance their resolution. However, these methods tend to produce blurry images. GANs, known to facilitate the generation of sharp, realistic looking images, provide the means to mitigate this problem. A variety of works have recognized this potential and proposed different ways to exploit GANs for denoising images with perceptually higher quality.

Table 16: De-noising GAN-based methods in medical image processing

method	Arch	loss	modality	dataset	performance	PR	code
Wolterink et al. (2017b)	CNN, GAN	CNN, Adv	CT (phantom) (cardiac)	unknown Train:48 Train:28	Agatston Score: Median=20.7 Min=6.1 Max=145.1	Yes	No
Wang et al. (2018)	U-net, ResNet, cGAN	Adv, L1	CT (ear)	unknown Train:14346 Test:74	P2PEs: Median=0.409 STD=0.133 Max=0.912	Yes	No
Yang et al. (2018)	WGAN, VGG	features distance, WGAN	CT	unknown Train:4000	Noise Suppression=3.20±0.25 Artifact Reduction=3.45±0.25 Overall Quality=3.70±0.15	Yes	No
Yi and Babyn (2018) SAGAN	MGAN, ResNet	Pixel-wise, MGAN, Sharpness	CT	CT phantom (Catphan 600) Train:4×708 Test:4×142	(N=10 ⁴) PSNR=26.77 SSIM=0.8454 (N=10 ⁵) PSNR=28.25 SSIM=0.87	Yes	No

For example, Wolterink et al. (2017b) propose to learn tissue texture information from a small amount of paired data and address the blurring effect using GANs. Similarly, Wang et al. (2018) propose to use the cGAN to remove metal artifacts from CT images. Yang et al. (2018) utilize a combination of the W-GAN and a perceptual loss to improve training stability without losing perceptual quality. The sharpness of the denoised image is also the factor that Yi and Babyn (2018) (Sharpness Aware Generative Adversarial Network - SAGAN) worked on (Figure 11).

Table 16 summarizes major GAN-based denoising methods. While visually, the results look compelling, it seems that an adequate, objective metric to evaluate the strength of methods in preserving important medical information of the image is not available yet. As PSNR, MSE, SSIM, SD, and mean - the most commonly used metrics in the evaluation of de-noising methods - are not sensitive enough to recognize texture details, the RoI of any image should be segmented to be measured by metrics, which is an expensive procedure. The introduction of a new, meaningful metric is subject to future work. Despite this limitation, visually results achieved in reviewed papers benefit from the ability of GANs in learning the main general features of a domain of images. Also by modifying the loss function to consider more textural features, good performance in medical image de-noising is demonstrated. However, finding a faster and more accurate framework is an open direction to be worked on in the future.

4.6. Registration

Traditional registration methods suffer from parameter dependency and heavy optimization load. CNNs have been successfully used to align medical images in a single forward-pass through the network. Therein, GANs with their excellent image transformation capabilities have emerged as a candidate to extract a more optimal registration mapping.

Fan et al. (2018) propose an unsupervised GAN to register structural patterns (defined in patches) among different brain images. In 3D prostate MRI and intra-procedural Transrectal Ultrasound (TRUS), Yan et al. (2018) and Hu

et al. (2018) propose GANs for registration and deformation correction respectively. In the method proposed by Yan et al. (2018), the discriminator serves as a certainty evaluator during testing.

Table 17 summarizes properties of the mentioned methods and their performance. In registration tasks both local and global features are of importance. Since GANs learn features at various scales to model the discrepancy between distributions, they provide this beneficial information. While GANs significantly enhance the performance of registration methods, in some real medical settings the required performance can still not be reached.

Table 17: Registration GAN-based methods in medical image processing

method	Arch	loss	modality	dataset	performance	PR	code
Fan et al. (2018)	U-net, GAN	Adv, Regular	MRI 3D Brain	LPBA40, IBSR18, CUMC12, MGH10 Train:30 Test:10	DSC=71.8±2.3% DSC=57.8±2.7% DSC=54.4±2.9% DSC = 61.7±2.1%	Yes	No
Yan et al. (2018)	CNN, WGAN	Adv	Prostate 3D MRI and TRUS	unknown Train:636 Test:127	TRE = 3.84 mm DSC = 0.58	Yes	No
Hu et al. (2018)	3D GAN	Adv, DSC, Regular	Prostate 3D MRI TRUS	unknown 108 pairs	TRE = 6.3 mm DSC = 0.82	Yes	No

4.7. Classification

CNNs, known as the best performing classifiers, require a huge amount of training data. However, difficulties in access to medical data hampers their effective employment. The ability of GANs to augment the training data and to extract domain-specific features of every class can potentially help to overcome this limitation.

For separating useful from non-informative images in cardiac Ultra-Sound (US), Zhang et al. (2017a) propose the Semi-Coupled GAN (SCGAN). In this work, two generators are employed to generate useful and non-informative cardiac samples; The discriminator is extended to differentiate both real/fake and useful/non-informative samples (Figure 12).

For classification of prostate histopathology images into two Gleason grades, Ren et al. (2018) propose a GAN to extract features of every class and classify input patches based on those features. They also introduce a classification loss to prevent the network from classifying patches of the same image in the different Gleason grades.

Table 18 provides insights into the performance and summarizes properties of the mentioned methods. The results indicate that the classification tasks benefit from the GAN-generated samples.

5. Discussion

GANs have been receiving significant attention from the medical imaging community - this is evident from the sudden spike in the number of papers published using GANs.

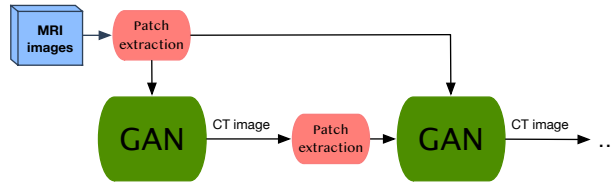


Figure 7: Synthesis: Proposed architecture by Quan et al. (2017)

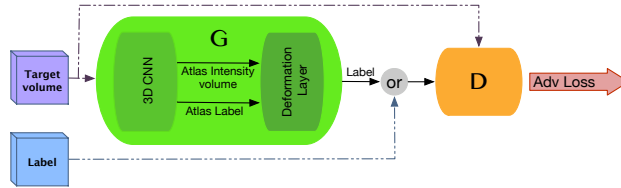


Figure 8: Segmentation: Proposed architecture by Dong et al. (2018)

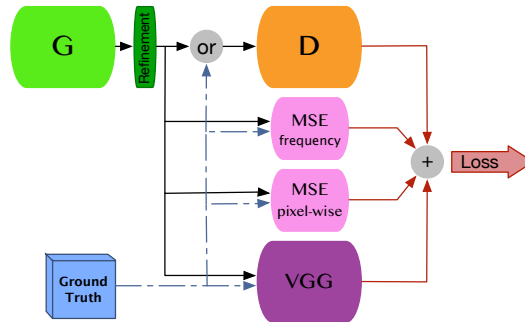


Figure 9: Reconstruction: DAGAN architecture (Yang et al., 2017b)

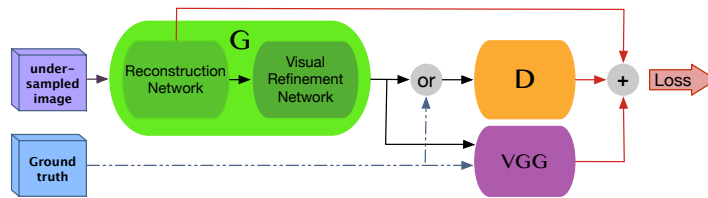


Figure 10: Reconstruction Proposed architecture by Seitzer et al. (2018)

Table 18: Classification GAN-based methods in medical image processing

method	Arch	loss	modality	dataset	performance	PR	code
Zhang et al. (2017a) SCGAN	GAN	Adv	MR (Cardiac)	UKBB 3400	(MAS - MBS) Acc=92.5, 89.3 Precision=87.6, 89.1 Recall=90.5, 91.7	Yes	No
Ren et al. (2018)	Su et al. (2013), GAN	Adv, patch-class	prostate histopathology	TCGA, CINJ	(TCGA/TCGA to CINJ) Accuracy = 0.77, 0.75	Yes	No

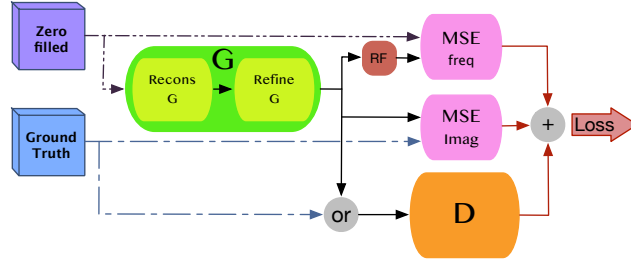


Figure 10: Reconstruction: RefineGAN architecture (Quan et al., 2017)

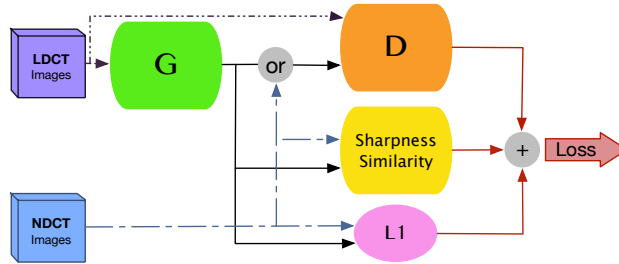


Figure 11: Denoising: SAGAN architecture (Yi and Babyn, 2018)

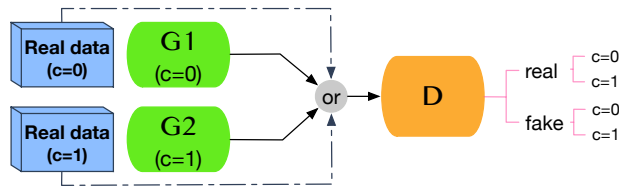


Figure 12: Classification: SCGAN architecture (Zhang et al., 2017a)

5.1. Advantages

They are capable of mimicking data distributions, producing realistic looking images and learning rich similarity metrics - which are beneficial for discriminative deep learning frameworks.

Scarcity of labeled data and class imbalance: Often times, annotations are expensive to obtain in medical imaging. This impairs supervised deep learning methods. At the same time, medical data often suffers from class imbalance, due to the rare nature of some pathologies. The ability of GAN in generating realistic looking images not only can be employed to enlarge training datasets but also it can be exploited in semi- and unsupervised settings. Great success has been made in image-to-image translation for cross-modality image synthesis, such as mapping from MR to CT data. By synthesizing across modalities, conditional GANs reduce the cost and risk factors of medical image acquisition (Section 4.1.2), and can offer multi-modal information which can be fused for better diagnostic decision making. In Unsupervised realms, the GAN’s ability to learn data distributions opens up the possibility to detect unseen abnormal cases in real datasets (Section 4.4).

Rich feature extraction: Learning distinctive patterns in medical images plays a vital role in the diagnosis of diseases. GANs, equipped with the adversarial training concept, are powerful in extracting semantically meaningful features from images which traditional pixel-wise losses fail to grasp. This property has been successfully leveraged in segmentation (Section 4.2), registration (Section 4.6), and de-noising (Section 4.5). On the other hand, the hierarchical discriminative potential of GANs has also been utilized for classification applications (Section 4.7).

5.2. Drawbacks

We identify three major drawbacks in the current form of GANs that might hinder their acceptance in the medical community:

Trustability of the Generated Data: In healthcare, where gaining the clinicians trust is the biggest challenge for any technology, images generated by GANs provide little comfort. The basic networks (generator and discriminator) are still deep neural networks, the mechanism of which is not sufficiently understood. In medical images intensities are typically associated with some meanings, e.g. in CT data every intensity can be mapped to the Hounsfield-scale and thus characterizes certain tissue. Such an association and mapping is currently missing from the GAN reconstruction - a shortcoming severe enough for clinicians to distrust images synthesized with GANs. In Computer Vision, where the overall perception is the main concern, these results are more adequate.

Unstable Training: The typical GAN training is unstable because of numerical and conceptual reasons (Creswell et al., 2018). This may result in convergence issues such as mode collapse or mode-hopping. Fundamental theoretical work focuses on solving this problem and usually provides benchmarks on Computer Vision Datasets, where generated images are easy to interpret. However, in medical imaging, where the modes of images are unclear, the identification of such unstable situations and unrealistic results can be very challenging. In the reviewed methods, architectural modifications and customized loss functions are proposed to address these problems. Yet, there is a lack of

proper evaluation tools and medical benchmarks which measure the efficacy of the proposed methods in a comparable way.

Evaluation: In medical imaging, researchers mostly rely on traditional pixel-wise metrics to evaluate GANs performance. This is tricky since GANs overcome the limitations of these traditional measures. Most of these metrics are usable only when ground truth images are available and this challenges the evaluation of unsupervised methods. On the other hand, as Lucic et al. (2018) mentioned, specific metrics should be employed to evaluate the performance of GAN-based methods due to the randomness of the initialization/optimization procedure and model instability problem. In the reviewed papers such a metric is not explored.

Uninterpretability: A model will be reliable in a medical environment if it follows features that clinicians consider in diagnosis and prognosis. Even if a model provides information which is not simply recognized by medical experts, reasons for its decision should be interpretable. While GANs show superior performance in many applications, they suffer from the same un-interpretability as other deep models. This is the main obstacle to their practical application in medical environments. Generally, Solving the interpretability of deep networks would open up a new direction to discover shortages in the models.

We believe GANs need to address the significant drawbacks discussed before being considered a trustworthy technology in practical medical image analysis. To this end, we can think of GANs as a technical building block rather than a stand-alone piece of technology for the future. For example, in the case of synthesizing CT data, enveloping GANs synthesis with a physics-based simulation might ensure realistic HU values. Training instabilities need to be addressed as well, which means rigorous experimentation to understand the convergence of GANs in the medical imaging context. Important steps have already been made in the Computer Vision field. In short, along with exciting results, GANs open up many possible research questions for the next few years. Proper understanding and answering those hold the key to their successful deployment in the real clinical scenario.

References

References

Barbara André, Tom Vercauteren, Anna M Buchner, Michael B Wallace, and Nicholas Ayache. A smart atlas for endomicroscopy using automated video retrieval. *Medical image analysis*, 15(4):460–476, 2011.

Assaf Arbel and Tammy Riklin-Raviv. Microscopy cell segmentation via adversarial neural networks. *2018 IEEE 15th International Symposium on Biomedical Imaging (ISBI 2018)*, pages 645–648, 2018.

Martín Arjovsky, Soumith Chintala, and Léon Bottou. Wasserstein gan. *CoRR*, abs/1701.07875, 2017.

- Christian F Baumgartner, Lisa M Koch, Kerem Can Tezcan, Jia Xi Ang, and Ender Konukoglu. Visual feature attribution using wasserstein gans. In *Proceedings of the IEEE Conference on Computer Vision and Pattern Recognition*, pages 8309–8319, 2018.
- Christoph Baur, Shadi Albarqouni, and Nassir Navab. Generating highly realistic images of skin lesions with gans. *arXiv preprint arXiv:1809.01410*, 2018a.
- Christoph Baur, Shadi Albarqouni, and Nassir Navab. Melanogans: High resolution skin lesion synthesis with gans. *CoRR*, abs/1804.04338, 2018b.
- Christoph Baur, Benedikt Wiestler, Shadi Albarqouni, and Nassir Navab. Deep autoencoding models for unsupervised anomaly segmentation in brain mr images. *arXiv preprint arXiv:1804.04488*, 2018c.
- Neslihan Bayramoglu, Mika Kaakinen, Lauri Eklund, and Janne Heikkilä. Towards virtual h&e staining of hyperspectral lung histology images using conditional generative adversarial networks. *2017 IEEE International Conference on Computer Vision Workshops (ICCVW)*, pages 64–71, 2017.
- Avi Ben-Cohen, Eyal Klang, Stephen P Raskin, Michal Marianne Amitai, and Hayit Greenspan. Virtual pet images from ct data using deep convolutional networks: Initial results. In *International Workshop on Simulation and Synthesis in Medical Imaging*, pages 49–57. Springer, 2017.
- Aïcha Bentaieb and Ghassan Hamarneh. Adversarial stain transfer for histopathology image analysis. *IEEE Transactions on Medical Imaging*, 37(3):792–802, 2018.
- Camilo Bermudez, Andrew J Plassard, Larry T Davis, Allen T Newton, Susan M Resnick, and Bennett A Landman. Learning implicit brain mri manifolds with deep learning. *arXiv preprint arXiv:1801.01847*, 2018.
- Lei Bi, Jinman Kim, Ashnil Kumar, Dagan Feng, and Michael Fulham. Synthesis of positron emission tomography (pet) images via multi-channel generative adversarial networks (gans). In *Molecular Imaging, Reconstruction and Analysis of Moving Body Organs, and Stroke Imaging and Treatment*, pages 43–51. Springer, 2017.
- Agisilaos Chartsias, Thomas Joyce, Rohan Dharmakumar, and Sotirios A Tsafaris. Adversarial image synthesis for unpaired multi-modal cardiac data. In *International Workshop on Simulation and Synthesis in Medical Imaging*, pages 3–13. Springer, 2017.
- Agisilaos Chartsias, Thomas Joyce, Giorgos Papanastasiou, Scott Semple, Michelle Williams, David E. Newby, Rohan Dharmakumar, and Sotirios A. Tsafaris. Factorised spatial representation learning: Application in semi-supervised myocardial segmentation. In *MICCAI*, 2018.

- Hao Chen, Xiaojuan Qi, Lequan Yu, and Pheng-Ann Heng. Dcan: Deep contour-aware networks for accurate gland segmentation. *2016 IEEE Conference on Computer Vision and Pattern Recognition (CVPR)*, pages 2487–2496, 2016.
- Liang-Chieh Chen, George Papandreou, Iasonas Kokkinos, Kevin Murphy, and Alan L. Yuille. Deeplab: Semantic image segmentation with deep convolutional nets, atrous convolution, and fully connected crfs. *IEEE Transactions on Pattern Analysis and Machine Intelligence*, 40:834–848, 2018a.
- Liang-Chieh Chen, George Papandreou, Iasonas Kokkinos, Kevin Murphy, and Alan L. Yuille. Deeplab: Semantic image segmentation with deep convolutional nets, atrous convolution, and fully connected crfs. *IEEE Transactions on Pattern Analysis and Machine Intelligence*, 40:834–848, 2018b.
- Xiaoran Chen and Ender Konukoglu. Unsupervised detection of lesions in brain mri using constrained adversarial auto-encoders. *CoRR*, abs/1806.04972, 2018.
- Yuhua Chen, Feng Shi, Anthony G Christodoulou, Yibin Xie, Zhengwei Zhou, and Debiao Li. Efficient and accurate mri super-resolution using a generative adversarial network and 3d multi-level densely connected network. In *International Conference on Medical Image Computing and Computer-Assisted Intervention*, pages 91–99. Springer, 2018c.
- Hyunjoo Cho, Sungbin Lim, Gunho Choi, and Hyunseok Min. Neural stain-style transfer learning using gan for histopathological images. *CoRR*, abs/1710.08543, 2017.
- Maria J. M. Chuquicusma, Sarfaraz Hussein, Jeremy R Burt, and Ulas Bagci. How to fool radiologists with generative adversarial networks? a visual turing test for lung cancer diagnosis. *2018 IEEE 15th International Symposium on Biomedical Imaging (ISBI 2018)*, pages 240–244, 2018.
- Joseph Paul Cohen, Margaux Luck, and Sina Honari. Distribution matching losses can hallucinate features in medical image translation. *arXiv preprint arXiv:1805.08841*, 2018.
- Pedro Costa, Adrian Galdran, Maria Inês Meyer, Michael David Abràmoff, Meindert Niemeijer, Ana Maria Mendona, and Aurélio Campilho. Towards adversarial retinal image synthesis. *CoRR*, abs/1701.08974, 2017a.
- Pedro Costa, Adrian Galdran, Maria Ines Meyer, Meindert Niemeijer, Michael Abràmoff, Ana Maria Mendonça, and Aurélio Campilho. End-to-end adversarial retinal image synthesis. *IEEE transactions on medical imaging*, 2017b.
- Antonia Creswell, Tom White, Vincent Dumoulin, Kai Arulkumaran, Biswa Sengupta, and Anil A Bharath. Generative adversarial networks: An overview. *IEEE Signal Processing Magazine*, 35(1):53–65, 2018.

- Wei Dai, Nanqing Dong, Zeya Wang, Xiaodan Liang, Hao Zhang, and Eric P Xing. Scan: Structure correcting adversarial network for organ segmentation in chest x-rays. In *Deep Learning in Medical Image Analysis and Multimodal Learning for Clinical Decision Support*, pages 263–273. Springer, 2018.
- Suyu Dong, Gongning Luo, Kuanquan Wang, Shaodong Cao, Ashley Mercado, Olga Shmuilovich, Henggui Zhang, and Shuo Li. Voxelatlasgan: 3d left ventricle segmentation on echocardiography with atlas guided generation and voxel-to-voxel discrimination. In *International Conference on Medical Image Computing and Computer-Assisted Intervention*, pages 622–629. Springer, 2018.
- Jingfan Fan, Xiaohuan Cao, Zhong Xue, Pew-Thian Yap, and Dinggang Shen. Adversarial similarity network for evaluating image alignment in deep learning based registration. In *International Conference on Medical Image Computing and Computer-Assisted Intervention*, pages 739–746. Springer, 2018.
- Maayan Frid-Adar, Eyal Klang, Michal Amitai, Jacob Goldberger, and Hayit Greenspan. Synthetic data augmentation using gan for improved liver lesion classification. *2018 IEEE 15th International Symposium on Biomedical Imaging (ISBI 2018)*, pages 289–293, 2018.
- Ben Glocker, Darko Zikic, Ender Konukoglu, David R Haynor, and Antonio Criminisi. Vertebrae localization in pathological spine ct via dense classification from sparse annotations. In *International Conference on Medical Image Computing and Computer-Assisted Intervention*, pages 262–270. Springer, 2013.
- Ian Goodfellow, Jean Pouget-Abadie, Mehdi Mirza, Bing Xu, David Warde-Farley, Sherjil Ozair, Aaron Courville, and Yoshua Bengio. Generative adversarial nets. In *Advances in neural information processing systems*, pages 2672–2680, 2014a.
- Ian J Goodfellow, Jonathon Shlens, and Christian Szegedy. Explaining and harnessing adversarial examples. *arXiv preprint arXiv:1412.6572*, 2014b.
- John T. Guibas, Tejpal S. Virdi, and Peter S. Li. Synthetic medical images from dual generative adversarial networks. *CoRR*, abs/1709.01872, 2017.
- Liang Han and Zhaozheng Yin. Transferring microscopy image modalities with conditional generative adversarial networks. In *Proceedings of the IEEE Conference on Computer Vision and Pattern Recognition Workshops*, pages 99–107, 2017.
- Liang Han and Zhaozheng Yin. A cascaded refinement gan for phase contrast microscopy image super resolution. In *MICCAI*, 2018.
- Yipeng Hu, Eli Gibson, Li-Lin Lee, Weidi Xie, Dean C Barratt, Tom Vercauteren, and J Alison Noble. Freehand ultrasound image simulation with spatially-conditioned generative adversarial networks. In *Molecular Imaging*,

- Reconstruction and Analysis of Moving Body Organs, and Stroke Imaging and Treatment*, pages 105–115. Springer, 2017.
- Yipeng Hu, Eli Gibson, Nooshin Ghavami, Ester Bonmati, Caroline M. Moore, Mark Emberton, Tom Vercauteren, J. Alison Noble, and Dean C. Barratt. Adversarial deformation regularization for training image registration neural networks. In *MICCAI*, 2018.
- Yuankai Huo, Zhoubing Xu, Shunxing Bao, Camilo Bermudez, Andrew J Plassar, Jiaqi Liu, Yuang Yao, Albert Assad, Richard G Abramson, and Bennett A Landman. Splenomegaly segmentation using global convolutional kernels and conditional generative adversarial networks. In *Medical Imaging 2018: Image Processing*, volume 10574, page 1057409. International Society for Optics and Photonics, 2018.
- Phillip Isola, Jun-Yan Zhu, Tinghui Zhou, and Alexei A. Efros. Image-to-image translation with conditional adversarial networks. *2017 IEEE Conference on Computer Vision and Pattern Recognition (CVPR)*, pages 5967–5976, 2017.
- Jue Jiang, Yu-Chi Hu, Neelam Tyagi, Pengpeng Zhang, Andreas Rimner, Gig S Mageras, Joseph O Deasy, and Harini Veeraraghavan. Tumor-aware, adversarial domain adaptation from ct to mri for lung cancer segmentation. In *International Conference on Medical Image Computing and Computer-Assisted Intervention*, pages 777–785. Springer, 2018.
- Dakai Jin, Ziyue Xu, Youbao Tang, Adam P Harrison, and Daniel J Mollura. Ct-realistic lung nodule simulation from 3d conditional generative adversarial networks for robust lung segmentation. *arXiv preprint arXiv:1806.04051*, 2018.
- Konstantinos Kamnitsas, Christian Baumgartner, Christian Ledig, Virginia Newcombe, Joanna Simpson, Andrew Kane, David Menon, Aditya Nori, Antonio Criminisi, Daniel Rueckert, et al. Unsupervised domain adaptation in brain lesion segmentation with adversarial networks. In *International Conference on Information Processing in Medical Imaging*, pages 597–609. Springer, 2017.
- Tero Karras, Timo Aila, Samuli Laine, and Jaakko Lehtinen. Progressive growing of gans for improved quality, stability, and variation. *arXiv preprint arXiv:1710.10196*, 2017.
- Boah Kim and Jong Chul Ye. Cycle-consistent adversarial network with polyphase u-nets for liver lesion segmentation. 2018.
- Andy Kitchen and Jarrel Seah. Deep generative adversarial neural networks for realistic prostate lesion mri synthesis. *CoRR*, abs/1708.00129, 2017.
- Simon Kohl, David Bonekamp, Heinz-Peter Schlemmer, Kaneschka Yaqubi, Markus Hohenfellner, Boris Hadaschik, Jan-Philipp Radtke, and Klaus H.

- Maier-Hein. Adversarial networks for the detection of aggressive prostate cancer. *CoRR*, abs/1702.08014, 2017.
- Avisek Lahiri, Kumar Ayush, Prabir Kumar Biswas, and Pabitra Mitra. Generative adversarial learning for reducing manual annotation in semantic segmentation on large scale microscopy images: Automated vessel segmentation in retinal fundus image as test case. *2017 IEEE Conference on Computer Vision and Pattern Recognition Workshops (CVPRW)*, pages 794–800, 2017.
- Christian Ledig, Lucas Theis, Ferenc Huszar, Jose Caballero, Andrew Cunningham, Alejandro Acosta, Andrew P. Aitken, Alykhan Tejani, Johannes Totz, Zehan Wang, and Wenzhe Shi. Photo-realistic single image super-resolution using a generative adversarial network. *2017 IEEE Conference on Computer Vision and Pattern Recognition (CVPR)*, pages 105–114, 2017a.
- Christian Ledig, Lucas Theis, Ferenc Huszár, Jose Caballero, Andrew Cunningham, Alejandro Acosta, Andrew P Aitken, Alykhan Tejani, Johannes Totz, Zehan Wang, et al. Photo-realistic single image super-resolution using a generative adversarial network. In *CVPR*, volume 2, page 4, 2017b.
- Chuan Li and Michael Wand. Precomputed real-time texture synthesis with markovian generative adversarial networks. In *European Conference on Computer Vision*, pages 702–716. Springer, 2016.
- Zeju Li, Yuanyuan Wang, and Jinhua Yu. Brain tumor segmentation using an adversarial network. In *International MICCAI Brainlesion Workshop*, pages 123–132. Springer, 2017a.
- Zeju Li, Yuanyuan Wang, and Jinhua Yu. Reconstruction of thin-slice medical images using generative adversarial network. In *International Workshop on Machine Learning in Medical Imaging*, pages 325–333. Springer, 2017b.
- Geert Litjens, Thijs Kooi, Babak Ehteshami Bejnordi, Arnaud Arindra Adiyoso Setio, Francesco Ciompi, Mohsen Ghafoorian, Jeroen AWM van der Laak, Bram van Ginneken, and Clara I Sánchez. A survey on deep learning in medical image analysis. *Medical image analysis*, 42:60–88, 2017.
- Mario Lucic, Karol Kurach, Marcin Michalski, Sylvain Gelly, and Olivier Brecheteau. Are gans created equal? a large-scale study. In *Advances in neural information processing systems*, pages 700–709, 2018.
- Dwarikanath Mahapatra, Behzad Bozorgtabar, Sajini Hewavitharanage, and Rahil Garnavi. Image super resolution using generative adversarial networks and local saliency maps for retinal image analysis. In *International Conference on Medical Image Computing and Computer-Assisted Intervention*, pages 382–390. Springer, 2017.
- Dwarikanath Mahapatra, Behzad Bozorgtabar, Jean-Philippe Thiran, and Mauricio Reyes. Efficient active learning for image classification and segmentation using a sample selection and conditional generative adversarial network. *arXiv preprint arXiv:1806.05473*, 2018.

- Xudong Mao, Qing Li, Haoran Xie, Raymond Y. K. Lau, Zhen Wang, and Stephen Paul Smolley. Least squares generative adversarial networks. *2017 IEEE International Conference on Computer Vision (ICCV)*, pages 2813–2821, 2017.
- Morteza Mardani, Enhao Gong, Joseph Y. Cheng, Shreyas S Vasanaawala, Greg Zaharchuk, Marcus T. Alley, Neil Thakur, Song Han, William J. Dally, John M. Pauly, and Lei Xing. Deep generative adversarial networks for compressed sensing automates mri. *CoRR*, abs/1706.00051, 2017.
- Michaël Mathieu, Camille Couprie, and Yann LeCun. Deep multi-scale video prediction beyond mean square error. *CoRR*, abs/1511.05440, 2015.
- Fausto Milletari, Nassir Navab, and Seyed-Ahmad Ahmadi. V-net: Fully convolutional neural networks for volumetric medical image segmentation. *2016 Fourth International Conference on 3D Vision (3DV)*, pages 565–571, 2016.
- Mehdi Mirza and Simon Osindero. Conditional generative adversarial nets. *CoRR*, abs/1411.1784, 2014.
- Pim Moeskops, Mitko Veta, Maxime W Lafarge, Koen AJ Eppenhof, and Josien PW Pluim. Adversarial training and dilated convolutions for brain mri segmentation. In *Deep Learning in Medical Image Analysis and Multimodal Learning for Clinical Decision Support*, pages 56–64. Springer, 2017.
- Dong Nie, Roger Trullo, Jun Lian, Caroline Petitjean, Su Ruan, Qian Wang, and Dinggang Shen. Medical image synthesis with context-aware generative adversarial networks. In *International Conference on Medical Image Computing and Computer-Assisted Intervention*, pages 417–425. Springer, 2017.
- Augustus Odena, Christopher Olah, and Jonathon Shlens. Conditional image synthesis with auxiliary classifier gans. In *ICML*, 2017.
- Sahin Olut, Yusuf Huseyin Sahin, Ugur Demir, and Gozde Unal. Generative adversarial training for mra image synthesis using multi-contrast mri. *arXiv preprint arXiv:1804.04366*, 2018.
- Chao Peng, Xiangyu Zhang, Gang Yu, Guiming Luo, and Jian Sun. Large kernel matters improve semantic segmentation by global convolutional network. *2017 IEEE Conference on Computer Vision and Pattern Recognition (CVPR)*, pages 1743–1751, 2017.
- Tran Minh Quan, Thanh Nguyen-Duc, and Won-Ki Jeong. Compressed sensing mri reconstruction with cyclic loss in generative adversarial networks. *CoRR*, abs/1709.00753, 2017.
- Alec Radford, Luke Metz, and Soumith Chintala. Unsupervised representation learning with deep convolutional generative adversarial networks. *CoRR*, abs/1511.06434, 2015.

- Daniele Ravì, Agnieszka Barbara Szczotka, Dzhoshkun Ismail Shakir, Stephen P. Pereira, and Tom Vercauteren. Adversarial training with cycle consistency for unsupervised super-resolution in endomicroscopy. 2018.
- Jian Ren, Ilker Hacihaliloglu, Eric A. Singer, David J. Foran, and Xin Qi. Adversarial domain adaptation for classification of prostate histopathology whole-slide images. In *MICCAI*, 2018.
- Mina Rezaei, Konstantin Harmuth, Willi Gierke, Thomas Kellermeier, Martin Fischer, Haojin Yang, and Christoph Meinel. A conditional adversarial network for semantic segmentation of brain tumor. In *BrainLes@MICCAI*, 2017.
- Olaf Ronneberger, Philipp Fischer, and Thomas Brox. U-net: Convolutional networks for biomedical image segmentation. In *International Conference on Medical image computing and computer-assisted intervention*, pages 234–241. Springer, 2015.
- Sajith Kecheril Sadanandan, Johan Karlsson, and Carolina Wählby. Spheroid segmentation using multiscale deep adversarial networks. *2017 IEEE International Conference on Computer Vision Workshops (ICCVW)*, pages 36–41, 2017.
- Irina Sánchez and Verónica Vilaplana. Brain mri super-resolution using 3d generative adversarial networks. 2018.
- Thomas Schlegl, Philipp Seeböck, Sebastian M Waldstein, Ursula Schmidt-Erfurth, and Georg Langs. Unsupervised anomaly detection with generative adversarial networks to guide marker discovery. In *International Conference on Information Processing in Medical Imaging*, pages 146–157. Springer, 2017.
- Maximilian Seitzer, Guang Yang, Jo Schlemper, Ozan Oktay, Tobias Würfl, Vincent Christlein, Tom Wong, Raad Mohiaddin, David Firmin, Jennifer Keegan, et al. Adversarial and perceptual refinement for compressed sensing mri reconstruction. In *International Conference on Medical Image Computing and Computer-Assisted Intervention*, pages 232–240. Springer, 2018.
- Anjany Sekuboyina, Markus Rempfler, Jan Kukacka, Giles Tetteh, Alexander Valentinitzsch, Jan S. Kirschke, and Bjoern H. Menze. Btrfly net: Vertebrae labelling with energy-based adversarial learning of local spine prior. *CoRR*, abs/1804.01307, 2018.
- M. Tarek Shaban, Christoph Baur, Nassir Navab, and Shadi Albarqouni. Staingan: Stain style transfer for digital histological images. *CoRR*, abs/1804.01601, 2018.
- Sharath M Shankaranarayana, Keerthi Ram, Kaushik Mitra, and Mohanasankar Sivaprakasam. Joint optic disc and cup segmentation using fully convolutional and adversarial networks. In *Fetal, Infant and Ophthalmic Medical Image Analysis*, pages 168–176. Springer, 2017.

- Ohad Shitrit and Tammy Riklin-Raviv. Accelerated magnetic resonance imaging by adversarial neural network. In *DLMIA/ML-CDS@MICCAI*, 2017.
- Ravid Shwartz-Ziv and Naftali Tishby. Opening the black box of deep neural networks via information. *CoRR*, abs/1703.00810, 2017.
- Jaemin Son, Sang Jun Park, and Kyu-Hwan Jung. Retinal vessel segmentation in fundoscopic images with generative adversarial networks. *CoRR*, abs/1706.09318, 2017.
- Hang Su, Zhaozheng Yin, Seungil Huh, and Takeo Kanade. Cell segmentation in phase contrast microscopy images via semi-supervised classification over optics-related features. *Medical image analysis*, 17 7:746–65, 2013.
- Christian Szegedy, Wojciech Zaremba, Ilya Sutskever, Joan Bruna, Dumitru Erhan, Ian J. Goodfellow, and Rob Fergus. Intriguing properties of neural networks. *CoRR*, abs/1312.6199, 2013.
- Ayco Tack, Amitava Mukhopadhyay, and Stefan Zachow. Knee menisci segmentation using convolutional neural networks: data from the osteoarthritis initiative. *Osteoarthritis and cartilage*, 26 5:680–688, 2018.
- Sotirios A. Tsafaris Thomas Joyce, Agisilaos Chartsias. Deep multi-class segmentation without ground-truth labels. 2018.
- Francis Tom and Debdoot Sheet. Simulating patho-realistic ultrasound images using deep generative networks with adversarial learning. *2018 IEEE 15th International Symposium on Biomedical Imaging (ISBI 2018)*, pages 1174–1177, 2018.
- Ahmet Tuysuzoglu, Jeremy Tan, Kareem Eissa, Atilla P Kiraly, Mamadou Diallo, and Ali Kamen. Deep adversarial context-aware landmark detection for ultrasound imaging. In *International Conference on Medical Image Computing and Computer-Assisted Intervention*, pages 151–158. Springer, 2018.
- Andreea Udrea and George Daniel Mitra. Generative adversarial neural networks for pigmented and non-pigmented skin lesions detection in clinical images. In *Control Systems and Computer Science (CSCS), 2017 21st International Conference on*, pages 364–368. IEEE, 2017.
- Jianing Wang, Yiyuan Zhao, Jack H Noble, and Benoit M Dawant. Conditional generative adversarial networks for metal artifact reduction in ct images of the ear. In *International Conference on Medical Image Computing and Computer-Assisted Intervention*, pages 3–11. Springer, 2018.
- Wenbin Wei, Emilie Poirion, Benedetta Bordini, Stanley Durrleman, Nicholas Ayache, Bruno Stankoff, and Olivier Colliot. Learning myelin content in multiple sclerosis from multimodal mri through adversarial training. *CoRR*, abs/1804.08039, 2018.

- Jelmer M Wolterink, Anna M Dinkla, Mark HF Savenije, Peter R Seevinck, Cornelis AT van den Berg, and Ivana Išgum. Deep mr to ct synthesis using unpaired data. In *International Workshop on Simulation and Synthesis in Medical Imaging*, pages 14–23. Springer, 2017a.
- Jelmer M Wolterink, Tim Leiner, Max A Viergever, and Ivana Išgum. Generative adversarial networks for noise reduction in low-dose ct. *IEEE transactions on medical imaging*, 36(12):2536–2545, 2017b.
- Jelmer M Wolterink, Tim Leiner, and Ivana Isgum. Blood vessel geometry synthesis using generative adversarial networks. *arXiv preprint arXiv:1804.04381*, 2018.
- Chenchu Xu, Lei Xu, Gary Brahm, Heye Zhang, and Shuo Li. Mutgan: Simultaneous segmentation and quantification of myocardial infarction without contrast agents via joint adversarial learning. In *MICCAI*, 2018.
- Yuan Xue, Tao Xu, Han Zhang, L. Rodney Long, and Xiaolei Huang. Segan: Adversarial network with multi-scale l1 loss for medical image segmentation. *Neuroinformatics*, pages 1–10, 2018.
- Pingkun Yan, Sheng Xu, Ardeshir R. Rastinehad, and Bradford J. Wood. Adversarial image registration with application for mr and trus image fusion. In *MLMI@MICCAI*, 2018.
- Dong Yang, Daguang Xu, S Kevin Zhou, Bogdan Georgescu, Mingqing Chen, Sasa Grbic, Dimitris Metaxas, and Dorin Comaniciu. Automatic liver segmentation using an adversarial image-to-image network. In *International Conference on Medical Image Computing and Computer-Assisted Intervention*, pages 507–515. Springer, 2017a.
- Guang Yang, Simiao Yu, Hao Dong, Greg Slabaugh, Pier Luigi Dragotti, Xujiang Ye, Fangde Liu, Simon Arridge, Jennifer Keegan, Yike Guo, et al. Dagan: Deep de-aliasing generative adversarial networks for fast compressed sensing mri reconstruction. *IEEE Transactions on Medical Imaging*, 2017b.
- Qingsong Yang, Pingkun Yan, Yanbo Zhang, Hengyong Yu, Yongyi Shi, Xuanqin Mou, Mannudeep K Kalra, Yi Zhang, Ling Sun, and Ge Wang. Low dose ct image denoising using a generative adversarial network with wasserstein distance and perceptual loss. *IEEE Transactions on Medical Imaging*, 2018.
- Xin Yi and Paul Babyn. Sharpness-aware low-dose ct denoising using conditional generative adversarial network. *Journal of Digital Imaging*, pages 1–15, 2018.
- Simiao Yu, Hao Dong, Guang Yang, Gregory G. Slabaugh, Pier Luigi Dragotti, Xujiang Ye, Fangde Liu, Simon R. Arridge, Jennifer Keegan, David N. Firmin, and Yike Guo. Deep de-aliasing for fast compressive sensing mri. *CoRR*, abs/1705.07137, 2017.

- Le Zhang, Ali Gooya, and Alejandro F Frangi. Semi-supervised assessment of incomplete lv coverage in cardiac mri using generative adversarial nets. In *International Workshop on Simulation and Synthesis in Medical Imaging*, pages 61–68. Springer, 2017a.
- Pengyue Zhang, Fusheng Wang, Wei Xu, and Yu Li. Multi-channel generative adversarial network for parallel magnetic resonance image reconstruction in k-space. In *International Conference on Medical Image Computing and Computer-Assisted Intervention*, pages 180–188. Springer, 2018.
- Yizhe Zhang, Lin Yang, Jianxu Chen, Maridel Fredericksen, David P. Hughes, and Danny Ziyi Chen. Deep adversarial networks for biomedical image segmentation utilizing unannotated images. In *MICCAI*, 2017b.
- He Zhao, Huiqi Li, and Li Cheng. Synthesizing filamentary structured images with gans. *CoRR*, abs/1706.02185, 2017.
- Miaoyun Zhao, Li Wang, Jiawei Chen, Dong Nie, Yulai Cong, Sahar Ahmad, Angela Ho, Peng Yuan, Steve H Fung, Hannah H Deng, et al. Craniomaxillofacial bony structures segmentation from mri with deep-supervision adversarial learning. In *International Conference on Medical Image Computing and Computer-Assisted Intervention*, pages 720–727. Springer, 2018a.
- Miaoyun Zhao, Li Wang, Jiawei Chen, Dong Nie, Yulai Cong, Sahar Ahmad, Angela S. P. Ho, Peng Yuan, Steve H. Fung, Hannah H. Deng, James J. Xia, and Dinggang Shen. Craniomaxillofacial bony structures segmentation from mri with deep-supervision adversarial learning. In *MICCAI*, 2018b.
- Jun-Yan Zhu, Taesung Park, Phillip Isola, and Alexei A. Efros. Unpaired image-to-image translation using cycle-consistent adversarial networks. *2017 IEEE International Conference on Computer Vision (ICCV)*, pages 2242–2251, 2017.